NASA Contract Report 166287

USAAVRADCOM TR 82-A-3

AEROELASTIC ANALYSIS OF THE ELASTIC GIMBAL ROTOR

Raymond G. Carlson
Wen-Liu Miao

Contract DAAK51-80-C-0016
May 1981

NASA Contractor Report 166287

USAAVRADCOM TR 82-A-3

AEROELASTIC ANALYSIS OF THE ELASTIC GIMBAL ROTOR

Raymond G. Carlson
Wen-Liu Miao
Sikorsky Aircraft
Division of United Technologies Corporation
Stratford, CT 06602

Prepared for
U.S. Army Research and Technology
Laboratories (AVRADCOM)
under Contract DAAK51-80-C-0016

National Aeronautics and
Space Administration

Ames Research Center
Moffett Field, California 94035

United States Army
Aviation Research and
Development Command
Research and Technology
Laboratory
Moffett Field, California 94035

PREFACE

The work reported herein was performed by Sikorsky Aircraft Division of United Technologies Corporation under Contract DAAK51-80-C-0016 for the Applied Technology Laboratory, U.S. Army Research and Technology Laboratories (AVRADCOM), Fort Eustis, Virginia. The work was carried out under the technical cognizance of Dr. Robert Ormiston of the Aeromechanics Laboratory, USARTL, and Patrick Cancro of the Applied Technology Laboratory. Sikorsky engineering personnel directly involved in the program include Dr. Raymond Carlson (Task Manager), Evan Fradenburgh, Wen-Liu Miao, Dr. Sesi Kottapali, and Albert T. Krauss. Dr. Richard Bielawa of United Technologies Research Center developed the computer program modifications necessary for this program.

TABLE OF CONTENTS

TABLE OF CONTENTS (Continued)

LIST OF ILLUSTRATIONS

LIST OF ILLUSTRATIONS (Continued)

LIST OF ILLUSTRATIONS (Continued)

1.0 INTRODUCTION

The Elastic Gimbal Rotor (EGR) is a new Sikorsky concept in helicopter rotor systems. The EGR uses essentially bearingless rotor blades attached to a rotor head which is able to tilt relative to the rotor shaft. The tilt motion about the gimbal bearing is restrained by an elastically deformable member or members which form part of the hub. This spring restraint action permits hub moments to be transferred from the rotor blades to the main rotor shaft. The concept combines advantages of other rotor systems with several unique capabilities of its own. The bearingless rotor blades simplify the basic rotor hub to reduce hub weight. The design of the spring members provides the capability to select the desired control power or hub moment stiffness. The use of a gimbal bearing replaces blade flapping with hub tilt and lowers the Coriolis-induced loads. This configuration makes blade dynamics less important to the basic aircraft control dynamics than a conventional "hingeless" rotor would, so that a wider range of blade stiffness can be considered.

This program was a preliminary study of the elastic gimbal rotor. The emphasis was on the dynamic loads and the aeroelastic response of the system. The basic load paths on the inboard end of the blade and in the hub were investigated briefly, and the critical areas were analyzed using simplified analyses, thus providing a clearer understanding of the needs for designing a flightworthy rotor system. The aeroelastic analysis made use of an appropriately modified version of a coupled rotor airframe aeroelastic analysis developed by United Technologies Research Center. This program, called G400, was used to evaluate the rotor system on an airframe in hover and forward flight as well as on the ground (for ground resonance). Both soft inplane and stiff

inplane rotors were considered to explore the stiffness requirements for the EGR.

The following sections discuss the results of this study and show that the EGR has the potential to be a very significant development in rotor system technology.

2.0 THE ELASTIC GIMBAL ROTOR CONCEPT

The Sikorsky elastic gimbal rotor concept has the potential of substantially improving many rotor system attributes compared to existing rotors. It is basically a hingeless rotor attached to the rotor shaft through a gimbal. A spring with selected stiffness across the gimbal can provide desirable control moment characteristics between rotor and airframe while also serving as a rotor head fairing to minimize hub drag. The use of a gimbal practically eliminates one-per-rev blade flapping and thus reduces inplane Coriolis forces and the resulting inplane blade vibratory moments. This simplifies the design requirements for a hingeless rotor blade. Figure 1 shows the concept in its most basic form; Figure 2 shows one of a series of preliminary design iterations for this rotor concept.

The heart of the idea is the ability of the rotor head to tilt relative to the shaft, with elastic restraint to provide a constant speed universal joint without mechanical complexity. This is accomplished by having a hub structure that keeps the blades equally spaced and by having three or more blades. The flexible portions of the hub provide the desired spring restraint and also the torque transfer between shaft and blades. Blade lift is transferred from the center of the hub to the shaft through a single limited-motion spherical bearing which might be an elastomeric bearing in practice. This lift load, normally far less than the centrifugal force of a single blade, is easily accommodated. Blade centrifugal forces are carried through the central hub structure and are balanced by the other blades. Blade pitch motion can be

accommodated by a torsionally flexible blade root region, with an internal torque tube to transfer the pitching moments between control horn and outer blade.

The hub tilt degree of freedom afforded by the elastic gimbal greatly minimizes blade flapping relative to the hub for any given amount of tip path plane inclination relative to the shaft. This suppression of flapping motion minimizes the Coriolis effects which result from blade motion relative to the plane of constant rotational speed, as illustrated in Figure 3. Thus, the elastic gimbal rotor is expected to have some fundamental stress and vibration advantages over conventional so-called hingeless or bearingless rotors. Another potential virtue is that the rotor blades may be made relatively stiff in flatwise bending, avoiding critical stress concentration situations while still having a low rotor equivalent flapping hinge offset which will reduce high speed gust response and fundamental vibration excitation levels. The stiff blades also permit rotor startup or shutdown operations in high wind conditions without encountering excessive blade motion excursions or requiring the complexity of a blade flapping lock system at low rotational speeds. The reduced Coriolis motion of the blade also allows the consideration of a lightweight blade design which is stiff inplane, i.e., having the first inplane frequency above one-per-revolution, thus eliminating ground resonance concerns.

The elastic gimbal hub concept lends itself to the achievement of low hub weight, low-cost fabrication, low hub drag, and good aerodynamics in the blade root area, factors vital to any high-speed helicopter application.

The elastic gimbal rotor (EGR) shown in Figure 4 illustrates the fundamental components of the concept. The EGR shown consists of a main rotor shaft with a spherical elastomeric gimbal bearing attached to its upper end. The gimbal bearing is then attached to the central rotor hub member. The four blades are joined to the central hub at the root end of a torsionally flexible structure at the inboard end of the blades. Blade pitch is provided through a torque tube located internal to the blade root structure. The torque tube connects to the blade at its outboard end and is restrained at its inner end by a spherical pivot bearing between the torque tube and the hub. Blade pitch inputs are provided by a pushrod through a pitch horn connected to the torque tube near its inner end. A gimbal spring is connected between the rotor shaft and the four blades. The gimbal spring can be in a variety of forms; the illustration shows a circular disc with a rim which curls up at the outer end. This outer end is attached to the blade by means of a yoke. A removable dome-shaped cover is mounted on an attachment ring which in turn is joined to the gimbal spring.

The basic load paths in the hub region are well defined. Centrifugal forces in the blades are reacted against each other through the central hub member. Rotor thrust is transferred from the blade to the central hub and then through the gimbal bearing to the rotor shaft. The driving torque for the rotor goes from the rotor shaft through the gimbal spring to the rotor blades. Hub (rolling and pitching) steady moments are transferred from the blades to the rotor shaft through the gimbal spring. Pushrod loads are reacted against the hub to provide a pure torsional moment input to the blade torque tube for pitch change. Loads will be discussed further in Section 3.

3.0 LOADS ANALYSIS

The elastic gimbal rotor is still in the concept development phase and many design details are not yet available. Therefore, the stress and load distributions cannot be defined with any great accuracy. However, from the study of the concept of the EGR, the significant load paths and the approximate loadings can be determined. The previous section defined the function of each of the rotor system components, and the loads that act on the components. This section takes a more quantitative look at the loads and structural requirements. Four components are considered: the gimbal spring, the gimbal bearing, the flexible beams in the blades, and the blade torque tube. These components are essential to the EGR concept and are subjected to loadings which are characteristic of an EGR. The other components can be considered typical of all rotor designs, and can be sized to meet load requirements of a particular design.

3.1 GIMBAL SPRING

The gimbal spring serves two purposes in carrying loads in the rotor system: it transfers torque from the main rotor shaft to the blades and provides the flexibility required to give the helicopter the proper hub moment constant, which is the hub moment per unit pitch or roll deflection of the hub. This hub moment is the primary requirement that affects the gimbal spring design.

3.1.1 Gimbal Spring Flexibility

The gimbal spring must provide the required flexibility and also have adequate strength to carry the hub moment loads. A very stiff spring could be readily provided, for the deflections or strains could be kept small for low stresses. Similarly, a very flexible spring could be readily designed, for the load carried by the spring would be small, again helping to keep stresses low. Designing for a stiffness which provides a desired level of control power characteristics is more difficult. In the final design of a gimbal spring, a finite element analysis will probably be necessary to optimize the geometry. For this study a basic beam analysis was used to calculate the requirements for a gimbal spring which provides hub moment characteristics similar to an articulated rotor.

The hub moments generated by an articulated rotor and an elastic gimbal rotor are compared in Figure 4. For an articulated rotor, the steady hub moment resulting from a tip path plane tilt relative to the shaft is approximately

$$M = \frac{b}{2} e F_c \sin a_{1s}$$

from which the hub moment constant is

$$K = \frac{M}{a_{is}} = \frac{b}{2} eF_c \qquad \text{for small } a_{1s}$$

For an elastic gimbal rotor, from Figure 4, the hub moment is

$$M = \frac{b}{2} VR_H$$

where V is the vertical shear reaction on each blade at the gimbal spring attachment radius, R_H. Writing this relation in terms of an equivalent flapping hinge offset, e_{eq}, and the tip path plane angle, γ_{TPP}, gives

$$M_A = \frac{b}{2} VR_H = \frac{b}{2} e_{eq} F_c \sin \gamma_{TPP}$$

or approximately

$$e_{eq} = \frac{VR_H}{F_c \gamma_{TPP}} = \left(\frac{VR_H}{F_c \gamma_H}\right) \left(\frac{\gamma_H}{\gamma_{TPP}}\right)$$

The tip path plane angle is greater than the hub tilt angle since blade flexibility gives additional flatwise deflection of the blades. However, for the design being considered, the tip path plane angle is not much greater than the hub tilt angle. The shear reaction force causes a moment in the gimbal spring and hub which is given by

$$M = V (R_H - r)$$

The hub moment constant is

$$K = \frac{M}{\gamma_{TPP}}$$

or approximately (when γ_{TPP} is nearly the same as γ_H)

$$K = \frac{M}{\gamma_H} = \frac{VR_H}{w/R_H} = \frac{VR^2_H}{w}$$

where w is the vertical deflection of the gimbal spring at its outer end attachment point. The structural design requirement for the gimbal spring is to provide the desired level of hub moment constant, i.e., degree of flexibility, with adequate fatigue strength.

The gimbal spring characteristics needed to meet these requirements were analyzed using beam analysis. From Figure 5, it was assumed that a 90 degree sector of the gimbal spring carries the load transmitted by one blade. The effective width of the beam is then a function of radius. Two effective widths can be defined: a "curved" width ($\pi r/2$) or a "straight" width ($2r$). The smaller value ($\pi r/2$) will be used. The beam thickness then becomes a function of the load and allowable stress. Using

$$\frac{I}{c} = \frac{\pi r t^2}{12}$$

and $M = V(R_H - r)$,

then

$$S = \frac{M}{I/c} = \frac{12\ V(R_H - r)}{\pi r t^2}$$

or $$\frac{St^2}{V} = \frac{12}{\pi}\left(\frac{R_H}{r} - 1\right)$$

The parameter St^2/V is a function of radius only. It is plotted in Figure 6. Thus, thickness is a function of radius and the load and stress allowable.

The rotor size considered during this brief study was representative of what might be used for a 10,000 pound gross weight helicopter. The Sikorsky S-76 helicopter is in this size category, and the design loads assumed are similar but not identical to design loads of that helicopter. Main rotor blade centrifugal force was assumed to be 30,000 pounds. The desired equivalent flapping hinge offset was assumed to be 10 inches or about 4 percent of rotor radius for a good compromise between good control power and low vibration characteristics. The maximum tip path plane angle, γ_{TPP}, is about 7 degrees, or approximated, a_{1s} = 7 degrees.

From this with four blades,

$$M_{max} = \frac{b}{2} eF_c \sin a_{ls} = 73,122 \text{ in-lb}$$

For the EGR spring, assuming R_H is 10% of rotor radius or 26.4 in.,

$$V = \frac{M_{max}}{\frac{b}{2} R_H} = 1385 \text{ lb.}$$

For an allowable stress of 40,000 psi, the required thickness can be calculated using Figure 6. The resulting thickness distribution is shown in Figure 7.

Using a material with a modulus of elasticity of 16×10^6 psi (such as titanium), an allowable strain at 40,000 psi is $\varepsilon = 0.0025$. Using this and the curvature relationship for the beam

$$\frac{1}{\rho} = \frac{d^2w}{dr^2} = \frac{M}{EI} = \frac{2\varepsilon}{t}$$

the curvature can be plotted and integrated to give slope and deflection. The results are shown in Figure 8. Note that the deflection at the outboard end of the gimbal spring corresponds to a hub tilt angle of about 7 deg, which was the assumed value in deriving the applied load. Thus this set of material properties gives a spring which approximates the required stiffness.

This analysis is preliminary and points out the requirements for a gimbal hub spring. Final design would require finite element analysis of the spring to define the stress and stiffness characteristics more accurately. This preliminary analysis indicates that it is feasible to design a gimbal spring that will provide the desired stiffness and strength characteristics.

3.1.2 Gimbal Spring Torque Transfer

The second function of the gimbal spring is to transfer steady torque from the rotor shaft to the blades. The blades are attached to the gimbal spring at its outer radius. For the assumed 10,000-lb helicopter with total installed power of 1300 HP driving a main rotor at a normal tip speed of 675 fps,

$$Q = \frac{550\ HP}{(\Omega R)/R} = \frac{550 \times 1300}{675/22} = 23304\ \text{ft-lb}$$

The steady inplane force per blade is then

$$F = \frac{Q}{bR_H} = \frac{23304}{4x2.2} = 2648\ \text{lb}$$

This force will react against the flexible beams which are at the inboard end of the blades. The force is less than 10% of the centrifugal force acting on the flexible beams at that radius, or equivalent to a steady lag deflection of about 5 degrees on an articulated rotor. This inplane shear will have to be accounted for in designing the gimbal-spring-to-blade attachment to distribute the load, but no particular difficulty is anticipated.

3.2 GIMBAL BEARING

The gimbal bearing reacts the lift force and drag or propulsive force acting on the main rotor. In addition, it allows for tilting of the rotor hub in the pitch and roll directions.

Since the gimbal spring provides the torque reaction, the deflections and loads in the yaw direction would only result from flexibility of the gimbal spring, blade root section, and central hub structure. These should be very small. The

gimbal bearing requirement can be met by an elastomeric bearing similar to the elastomeric bearing in the S-76 main rotor blade. That bearing reacts the full blade centrifugal force and accommodates motion in the blade pitch, flap, and lag degrees of freedom. A comparison of the load and motion requirements for the two elastomeric bearings indicates a much less demanding requirement for the EGR gimbal bearing than for the S-76 main rotor blade bearing with respect to both requirements. Therefore, no major design difficulties are expected with this bearing.

3.3 TORQUE TUBE

The torque tube provides the torque required to change blade pitch. The tube is attached at its outer end to the outboard blade spar. At its inner end, the torque tube is connected to the central hub member by means of a spherical pivot bearing which also allows the torque tube to slide axially. The torque tube is also connected near the inner end to a pushrod through a pitch horn. This is the source of the pitch input.

The design requirements for the torque tube include the following:

1. High torsional stiffness to transmit the pitch input.

2. Low bending stiffness relative to the torsionally flexible blade structure to minimize the blade bending moment carried by the torque tube.

3. Sufficient strength.

The torque tube used in the baseline analysis has a GJ value of 12 x 10^6 lb-in. Using graphite wrapped at 45 deg with shear modulus, G, of 4.5 x 10^6 psi, the torsional moment of inertia, J, is 2.667 in^4. This can be achieved with a torque tube having an outer diameter of 2.5 in. and an inner diameter of 1.86 in. This stiffness value gives a torsional blade natural frequency of 5.9p, and a static stiffness:

$$K = \frac{GJ}{l} = \frac{12 \times 10^6}{58} = 206{,}900 \ \frac{\text{in-lb}}{\text{rad}}$$

$$= 3611 \ \frac{\text{in-lb}}{\text{deg}}$$

For typical design pushrod loads of 650 lb steady and 910 lb vibratory and a 6.5-inch pitch horn, the steady stress is

$$\tau_s = \frac{Qd}{2J} = \frac{650 \times 6.5 \times 2.5}{2 \times 2.667} = 1980 \text{ psi}$$

and the vibratory stress is

$$\tau_V = \frac{910 \times 6.5 \times 2.5}{2 \times 2.667} = 2772 \text{ psi}$$

Both values are well below allowable stresses and are acceptable. The torsional windup due to the steady load would be 1.6 deg and due to the vibratory load ±1.2 deg.

3.4 BLADE FLEXIBLE BEAMS

While there are a number of configurations which could be used to provide the flexibility required for the root end of the blade, the dual flexible beam configuration seems particularly suited to the needs of the EGR. Unfortunately, the two-beam configuration with the torque tube is a redundant structure subjected to a number of loads and requires an

analytical study and methods which are beyond the scope of this contract. NASTRAN or other specialized blade structural analyses will be needed to design the beams for a flight-worthy rotor. In a design study and flight test demonstration of a bearingless main rotor (Reference 1), it was concluded that better analytical tools were needed for the two-beam configuration.

The loads to which the flexible beam are subjected are several: the centrifugal force of the blades; flatwise, edgewise, and torsional moments; and shear forces in both the flatwise and edgewise directions. Rotor torque is input at a point along the beams and the sharing of the resultant inplane force between blade beams depends on the relative flexibilities of the components contained within the yoke which attaches the blade to the gimbal spring.

The relative distribution of forces and moments in each flexible beam depends on the above loads and upon the choice of configuration geometry. Beam cross-sectional shape and area; the separation distance and angle between the two beams; precone, prelag, droop and built-in root end pitch; and structural twist will all affect the load distribution in the beams. Therefore, while an equivalent single beam is used in the aeroelastic analysis of the EGR, it is recognized that more detailed analytical work is required to define the actual structure which will provide the required dynamic properties and also satisfy the steady and vibratory stress requirements.

---

1. Dixon, P. G. C., DESIGN, DEVELOPMENT, AND FLIGHT TEST DEMONSTRATION OF THE LOADS AND STABILITY CHARACTERISTICS OF A BEARINGLESS MAIN ROTOR, Boeing Vertol Company, USAAVRADCOM-TR-80-D-3, Applied Technology Laboratory, U.S. Army Research and Technology Laboratories, Fort Eustis, Virginia, June 1980, AD A086754.

4.0 G400 ROTOR AEROELASTIC ANALYSIS

The computer program used to analyze the aeroelastic response of the elastic gimbal rotor is the G400 Rotor Aeroelastic Analysis developed by United Technologies Research Center. Certain modifications were required in this program to enable it to model the elastic gimbal rotor. Basically the changes involved the capability to include the gimbal hub degrees of freedom and the control system coupling resulting from the gimbal. The G400 program analyzes all blades of the rotor and also includes the response of the rotor hub and airframe, modeling them either as rigid bodies or as modal degrees of freedom. The program can be used for ground resonance and for hover or forward flight analysis.

This analysis is a multiblade, multipurpose computer program characterized by a rigorous modeling of large, nonlinear and time-varying structural twist. Although developed in response to the specialized requirements of composite bearingless rotors (see Reference 2), the dynamic equations developed for this analysis are sufficiently general for valid application to all conventional rotor systems (articulated, semi-articulated, teetering, gimballed and hingeless) as well as to propellers and wind turbines. The differential equations of blade bending (flatwise and

---

2. Bielawa, R.L., AEROELASTIC ANALYSIS FOR HELICOPTER ROTOR BLADES WITH TIME-VARIABLE NONLINEAR STRUCTURAL TWIST AND MULTIPLE STRUCTURAL REDUNDANCY - MATHEMATICAL DERIVATION AND PROGRAM USER's MANUAL, United Technologies Research Center, NASA Contractor Report CR-2638, Langley Research Center, National Aeronautics and Space Administration, Langley, Virginia, October 1976.

edgewise) and torsion are solved using a Galerkin procedure where the normal "uncoupled mode" shapes, their spanwise derivatives and the spanwise derivative of the blade (nonlinear) twist are approximately combined to describe the "coupled" blade deflections. The aerodynamic description includes the use of predetermined static airfoil data, constant or variable (multiple harmonic and spanwise variable) inflow, and unsteady dynamic stall data. Two types of solutions are available: eigensolutions of various linearized equation sets for coupled frequency and/or stability analysis purposes, and time-history solutions of the complete nonlinear equations for harmonic analysis and/or transient aeroelastic response calculation purposes. The EGR program has been modified for use in the time-history solution only, and this type of solution was used exclusively in this study.

The principal assumptions used to derive the basic differential equation of motion are as follows:

1. The rotor is rotating at a constant angular velocity, has finite hub impedance, and is in steady translational flight.

2. The blade elasticity is adequately described by the conventional (linear) beam bending and bar torsion characteristics described in Reference 3. Although the effects of the additional section constants B_1 and B_2

---

3. Houbolt, J.C., and Brooks, G.W., DIFFERENTIAL EQUATION OF MOTION FOR COMBINED FLAPWISE BENDING, CHORDWISE BENDING, AND TORSION OF TWISTED NON-UNIFORM ROTOR BLADES, NACA Report 1346, 1958.

described therein are usually considered to be negligible for helicopter applications, they are potentially important for accurately analyzing solid sectional, highly twisted propeller blades and/or wind turbines. To preserve consistency with the rigor applied to other aspects of structural twist and to achieve universality with such nonhelicopter rotor systems, these elastic section constants are retained in the full nonlinear formulation given in Reference 3.

3. The elastic (torsion) axis of the undeflected blade is a straight line. However, when deflected in bending, the elastic axis defines a space curve about which the local torsion deflections must take place.

4. The blade aerodynamic and structural twist distributions are nonlinear; additionally the structural twist of the flexbeam (bearingless rotor applications only) is time variable.

5. The total (integrated) angle of structural twist is negligible beyond second order; cases of large local twist rates over short sections of span can be considered, however.

6. Radial foreshortening of blade elements due solely to elastic deflections, in the absence of precone (or flapping) and prelag (or lagging), is adequately represented by a second-order function of flatwise bending.

7. The feathering axis is coincident with the elastic axis of the elastically undeformed blade.

8. The blade distributions of center of gravity, aerodynamic center and center of tension (intersection of flatwise and edgewise neutral axes) are, in general, noncoincident with the elastic axis.

9. The blade sections have finite thicknesswise mass, but the thicknesswise displacement of the section center of gravity away from the chordwise principal axis is negligible.

10. The airframe is modelled by rigid body degrees of freedom or by modes. Steady loads (gravity, airframe drag, tail rotor forces) may be applied.

11. While assumptions regarding the smallness of various quantities and products of these quantities are not generally required for the implementation of time-history solutions of the full nonlinear equations, they are required for effecting consistent linearized approximations for the eigensolutions. For this case, coefficients of the perturbational variables whose orders of magnitude exceed ε^2 are neglected. Here ε is an unspecified small number less than unity. The assumed orders of magnitude of the various pertinent quantities, as measured by ε, are given in Reference 2.

4.1 EXPANDED ELASTIC GIMBAL ROTOR MODELING

The modelling of the coupled rotor and airframe was modified to provide the additional degrees of freedom needed to define an elastic gimbal rotor configuration. These changes did not modify the blade modelling, but were restricted to the hub and airframe only. The changes consisted of adding gimbal rigid body pitch and roll degrees of freedom using inertia and stiffness terms to define the gimbal dynamics. These

gimbal terms were combined with six rigid body airframe degrees of freedom for hover and forward flight analysis, and combined with a rigid body airframe attached to the ground by means of springs and dampers to model ground resonance. In addition, blade pitch to gimbal motion coupling was added to define the change in blade pitch due to roll or pitch of the rotor head above the gimbal bearing.

The mathematical structuring of the coupled rotor/gimbal/ airframe system is shown below. The rotor and airframe equations are coupled together through the inertia matrix relating acceleration in the rotor modal degrees of freedom and in the hub and airframe degrees of freedom with the excitation forces.

The modifications to G400 for the EGR combined with the original capabilities of the program now permit the analysis of a coupled rotor/airframe system using several choices of models. These include use of the gimbal pitch and roll degrees of freedom, the rigid body airframe degrees of freedom, and the airframe modes, providing effective motion at the rotor hub. Table 1 summarizes the options which may now be used. Option 6a on the list is for ground resonance. Options 5 and 6 are used to analyze the EGR in hover and forward flight. Option 5 considers the EGR only, with no airframe motion. The gimbal spring is attached to ground. Option 6 adds a free-flying airframe modelled by six rigid body degrees of freedom.

Table 1.

G400 MODELLING OPTIONS FOR ELASTIC GIMBAL ROTOR

Option	Number of Degrees of Freedom Hub	Airframe
1	1-6 Explicit (using impedances)	-- --
2	--	6 Rigid Body (free flying)
3	1-10 Modal	1-6 Modal (combined with hub to total 1-16 modes)
4	1-10 Modal	6 Rigid Body
5	2 Elastic (using inertia and stiffness)	--
6	2 Elastic	6 Rigid Body
6a	2 Elastic	6 Rigid Body with spring/ damper attachment to ground
7	2 Elastic plus 8 Modal	6 Rigid Body

4.1.1 Mathematical Structuring

The basic form of solution is a time-history in which the accelerations of the blade, hub and airframe degrees of freedom are calculated from a set of nonlinear equations relating the inertia matrix, A, and the accelerations of the degrees of freedom, X, to the time-varying excitation forces, F. This is represented as

$$\left[\begin{array}{ccc|cc} All_1 & & & A12_1^{(1)} & A12_1^{(2)} \\ & All_2 & & & \\ & & \ddots & & \\ & & All_M & A12_M^{(1)} & A12_M^{(2)} \\ \hline kA12_1^{(1)T} & \cdots & kA12_M^{(1)T} & A22 & A23 \\ kA12_1^{(2)T} & \cdots & kA12_M^{(2)T} & A23^T & A33 \end{array}\right] \left\{\begin{array}{c} \ddot{X}_{BM} \\ \ddot{X}_{H1} \\ \ddot{X}_{H2} \end{array}\right\} = \left\{\begin{array}{c} F_{B1} \\ \vdots \\ F_{BM} \\ F_{H1} \\ F_{H2} \end{array}\right\}$$

$\left\{\ddot{X}_{BM}\right\}$ = vector of mth blade modal accelerations

$\left\{\ddot{X}_{H1}\right\}$ = 7 element vector of hub accelerations, usually Eulerian degrees of freedom (7th element is rotor speed degree of freedom)

$\left\{ \ddot{X}_{H2} \right\}$ = 1 to 10 element vector of "supplemental" hub (airframe) accelerations - either explicit Eulerian degrees of freedom or modal responses.

The total motion of the hub is given by

$$\left\{ \ddot{X}_{H} \right\} = [\Phi_1] \left\{ \ddot{X}_{H1} \right\} + [\Phi_2] \left\{ \ddot{X}_{H2} \right\}$$

Here Φ_1 and Φ_2 are transformation matrices relating the motions (accelerations) of the hub and airframe degrees of freedom to the accelerations of the hub.

The forcing functions are:

$\left\{ F_{BM} \right\}$ = modal generalized forces for mth blade (no modifications needed)

$\left\{ F_{H1} \right\}$ = excitations for 1st 7 hub degrees of freedom (modified as appropriate)

$\left\{ F_{H2} \right\}$ = excitations for supplemental hub responses (new)

The elements of the A matrix coupling the hub and airframe degrees of freedom and the summation of the hub and airframe degrees of freedom to define the net hub motion depend upon the model option used. For the majority of the EGR study, Options 5 and 6, which include the hub pitch and roll degrees of freedom with or without the airframe rigid body degrees of freedom, were used. Table 2 shows the characteristics of the various matrix elements for each of the program options. The full capability used for the EGR (Options 6 and 6a) contains a fairly full array of matrix terms to define the hub to airframe coupling.

Table 2.

MATRIX ELEMENT CHARACTERISTICS

Option	Matrix Element				
	Φ_1	Φ_2	A22	A23	A33
1	I	O	Diag.	O	I
2	I	O	Diag.	O	I
3	Non-I Nondiag.	Non-I Nondiag.	Diag.	O	Diag.
4	I	Non-I Nondiag.	Nondiag.	Finite	Diag.
5	I	Non-I Nondiag.	I	O	Non-I Nondiag.
6,6a	Non-I	Non-I Nondiag. (Time Depend)	Non-I Nondiag.	Non-I Nondiag.	Non-I Nondiag.
7	Non-I Nondiag.	Non-I Nondiag.	Non-I Nondiag.	Non-I Nondiag.	Diag. Except First 2 Elements

I = Identity Matrix

4.1.2 Rotor/Fuselage Coupling

The dynamic and aerodynamic coupling of the blades and hub to each other is accomplished using a "force-integration" approach. The velocities (relative to the air mass) and accelerations (relative to an inertial frame) of the appropriate differential elements of the blades are formulated to include those components occurring from hub motion. From these velocities and accelerations the total aerodynamic and inertial loads distribution on the blades is accurately simulated.

Similarly, the Euler angles of the hub are used to formulate the gravity load distributions. The six components of hub loading are also formed in this force-integration manner. These six hub load components are formed by appropriate integrations of the same blade load distributions (aerodynamic, inertial and gravity). These distributions also include contributions from the blade modal responses (deflections, rates and accelerations) to complete the full intercoupling between the blades and hub. The hub contributions to the inertial accelerations of the blade differential elements are typically nonlinear and highly periodic. For successful implementation of this approach, however, the terms involving the highest order differentiated terms must be explicitly extracted from the formulation to form the inertial coupling matrix at each time step. The formulations required to accomplish this implementation are inherent in internal calculation of the coupling matrix relating the accelerations given in the first equation in this section. The components of the total coupling matrix are time and blade deflection dependent and must therefore be calculated at each time step. Experience has further shown that the decoupling of the accelerations, as implied by the simultaneous equations solution of the acceleration equation,

at each time step is required to preclude one form of numerical instability.

4.1.3 Elements of the Inertia Matrix

The blade diagonal elements, (A11), are not changed in this version of G400. (See Reference 2 for original terms.) The hub/blade coupling matrix elements A12 are modified by the hub transformaton matrices Φ_1 and Φ_2.

Coupling matrices between the rotor blade modes and the hub and airframe modes are

$$\left[A12_M^{(1)}\right] = \left[A12_M\right] \left[\Phi_1\right]$$

$$\left[A12_M^{(2)}\right] = \left[A12_M\right] \left[\Phi_2\right]$$

where $A12_M$ is the rotating to nonrotating coordinate system inertia coupling matrix calculated in the original G400 program and k is a constant = $\frac{\overline{m}}{\pi\sigma\rho R^2}$

The (A23) coupling matrix is dependent on the type of supplemental hub degrees of freedom selected. For the EGR, the supplemental degrees of freedom are hub pitch and roll, and (A23) is a 7x2 matrix whose elements are dependent on the parameters peculiar to the EGR. If X_{H1} and X_{H2} are both to be pylon modal responses (Option 3), then the (A23) matrix is null, as the modes are orthogonal.

The fixed system diagonal matrix elements, (A22) and (A33),

are also configuration dependent. For Option 3, for example, (A22) and (A33) must be represented as diagonal matrices of generalized masses:

For this option, (A23) = 0, and

$$[A22] = \begin{bmatrix} M_1 & & & 0 \\ & \ddots & & \\ & & M_{N1} & \\ 0 & & & I_H \end{bmatrix} \qquad 1 \leq N1 \leq 6$$

and

$$[A33] = \begin{bmatrix} M_{N1+1} & & 0 \\ & \ddots & \\ 0 & & M_{N1+N2} \end{bmatrix} \qquad 1 \leq N2 \leq 10$$

A22 and A33 for the EGR are discussed in the following section.

4.1.4 EGR Matrix Elements

For the EGR, Option 6 is used with X_{H1} containing rigid body airframe degrees of freedom and X_{H2} containing the hub pitch and roll degrees of freedom. The hub motion participation matrices, Φ_1 & Φ_2 for Option 6 contain off-diagonal terms. Due to finite steady values of the gimbal deflection angles, θ_{XG} and θ_{yG}, the Φ_1 matrix must include nonzero off-diagonal terms. All nonzero elements are given below:

$$\left[\Phi_1\right] = \begin{bmatrix} 1 & 0 & 0 & 0 & -\theta_{YG} & 0 & 0 \\ 0 & 1 & 0 & 0 & \theta_{XG} & 0 & 0 \\ 0 & 0 & 1 & 0 & 0 & -\theta_{YG} & 0 \\ 0 & 0 & 0 & 1 & 0 & \theta_{XG} & 0 \\ \theta_{YG} & -\theta_{XG} & 0 & 0 & 1 & 0 & 0 \\ 0 & 0 & \theta_{YG} & -\theta_{XG} & 0 & 1 & 0 \\ 0 & 0 & 0 & 0 & 0 & 0 & 1 \end{bmatrix}$$

Note that Φ_1 is now time dependent, as θ_{XG} and θ_{YG} are system degrees of freedom, the gimbal motion relative to the airframe in the pitch and roll directions. Note also that here X_{H1} defines the airframe motion.

$$\left\{X_{H1}\right\} = \begin{Bmatrix} x \\ y \\ \theta_x \\ \theta_y \\ z \\ \theta_z \\ RPM \end{Bmatrix}$$

The Φ_2 matrix for the EGR is given as follows:

$$\left[\Phi_2\right] = \left[\begin{array}{cc|c} 0 & \bar{h}_G & \\ -\bar{h}_G & 0 & \\ 1 & 0 & \\ 0 & 1 & \\ \hline 0 & 0 & \\ | & | & \\ 0 & 0 & \end{array}\right]$$

Nominally null, except if additional supplementary modes are used.

Note that here X_{H2} defines the gimbal motion.

$$\{X_{H2}\} = \begin{Bmatrix} \theta_{xG} \\ \theta_{yG} \\ 0 \\ \vdots \\ 0 \end{Bmatrix}$$

Elements of inertia submatrices A23 and A33 for the EGR model are

$$[A33] = \left[\begin{array}{cc|c} \text{TEM42} & 0 & 0 \ldots 0 \\ 0 & \text{TEM42} & \\ \hline 0 & 0 & \\ \vdots & \vdots & \\ 0 & 0 & 0 \ldots 0 \end{array}\right]$$

$$[A23] = \left[\begin{array}{cc|c} 0 & \text{TEM41} & 0 \ldots 0 \\ -\text{TEM41} & 0 & \\ \text{TEM45} & 0 & \\ 0 & \text{TEM45} & \\ \hline 0 & 0 & \\ \vdots & \vdots & \\ 0 & 0 & 0 \ldots 0 \end{array}\right]$$

where

$$\text{TEM40} = \frac{C_{WGH}}{\sigma} \frac{\Omega^2 R}{g}$$

$$\text{TEM41} = \bar{Z}_{OGH} \ (\text{TEM40})$$

$$\text{TEM42} = I_{XHG} \ / R^5 \pi\sigma\rho$$

$$\text{TEM45} = \bar{Z}_{OGH} \ (\bar{Z}_{OGH} - \bar{h}_G) \ (\text{TEM40})$$

and

$$\bar{h}_G = h_G/R$$

$$\bar{Z}_{OGH} = Z_{OGH}/R$$

$$C_{WGH} = W_{GH}/\rho\pi R^2(\Omega R)^2$$

Special input terms required for the EGR are given below. The list includes those needed for the A23 and A33 matrix elements as well as additional terms defining the EGR configuration.

Term	Units
h_G, gimbal offset	in.
W_{GH}, weight of gimballed hub	lb
Z_{OGH}, c.g. distance above gimbal point	in.
I_{XGH}, inertia of W_{GH} about gimbal point	lb-sec^2-ft
I_{ZGH}, inertia of W_{GH} about rotation axis	lb-sec^2-ft
K_{EGR}, spring rate about gimbal point	lb-ft/rad
C_{EGR}, damper rate about gimbal point	lb-ft-sec/rad
r_{SA}, shell attachment radius	in.

4.1.5 A22 Matrix

The A22 matrix couples the primary hub degrees of freedom to each other directly. This coupling is determined by the nature of the support structure below and supporting the hub. The dimension of A22 is 7x7 and historically was used to provide the coupling between the hub degrees of freedom wherein these degrees of freedom consisted of the six explicit body-fixed (Eulerian) coordinates (three translations and three rotations) plus the rotor speed. Thus, this submatrix could be used to describe the inertia coupling

accruing from a rigid airframe or the general impedance characteristics of an elastic six-degree-of-freedom hub support pylon.

Matrix modifications were made to include the effects due to rotor mass and inertia in the deflected rotor state:

Define an incremental A22 matrix

$$[\Delta A22] = \begin{bmatrix} TEM\ 20 & 0 & 0 & \surd & 0 & \surd \\ 0 & TEM\ 20 & \surd & 0 & 0 & \surd \\ 0 & \surd & \surd & \surd & \surd & \surd \\ \surd & 0 & \surd & \surd & \surd & \surd \\ 0 & 0 & \surd & \surd & TEM\ 20 & 0 \\ \surd & \surd & \surd & \surd & 0 & \surd \end{bmatrix}$$

where checked terms represent nonzero values, which are deflection dependent. These terms are calculated in the original program. The matrix is taken to be symmetrical.

$$TEM20 = \frac{\Omega^2 R}{g} (NB) \frac{m_o}{\pi\rho\sigma R^2} \int_0^1 m dx$$

The A22, A23, A33 matrices are incremented as follows:

$$\left[A22\right] = \left[A22_o\right] + \left[\Phi_1\right]^T \left[\Delta A22\right] \left[\Phi_1\right]$$

$$\left[A23\right] = \left[A23_o\right] + \left[\Phi_1\right]^T \left[\Delta A22\right] \left[\Phi_2\right]$$

$$\left[A33\right] = \left[A33_o\right] + \left[\Phi_2\right]^T \left[\Delta A22\right] \left[\Phi_2\right]$$

where $[A22_o]$, $[A23_o]$, and $[A33_o]$ are matrices representing inertia of a "bladeless" hub. The forcing functions on the hub are

$$\left\{F_{H1}\right\} = \left[\Phi_1\right]^T \left\{\equiv_{HUB}\right\} + \left\{\equiv_{FUS}\right\}$$

$$\left\{F_{H2}\right\} = \left[\Phi_2\right]^T \left\{\equiv_{HUB}\right\} + \left\{\equiv_{GIMBAL}\right\}$$

where $\equiv_{HUB}$ are excitations due to rotor blade loads.

4.1.6 Forcing Functions

The $\equiv$ forcing function vectors represent the generalized excitations for each of the degrees of freedom. Consistent with the force-integration approach described under Rotor-Fuselage Coupling, these vectors represent appropriate integrations of the inertia, aerodynamic and gravity load distributions, but with the highest differentiated terms deleted. Additional terms can arise from the action of concentrated loads (from springs and dampers, etc.). Care must be taken to ensure that these concentrated loads are

boundary loads acting on a conceptually isolated dynamic degree of freedom and not internal loads. In this manner, double accounting of a given dynamic effect can be avoided.

4.1.7 Solution of Equations

The matrix equations are first rearranged to define the uncoupled hub and airframe accelerations in terms of the A matrix elements and the excitation forces. The blade modal accelerations are then calculated in terms of the matrix elements, excitation forces, and hub and airframe accelerations.

Blade accelerations:

$$\left\{\ddot{X}_{BM}\right\} = A11_M^{-1}\left[F_{BM} - A12_M\left(\left[\Phi_1\right]\ddot{X}_{H1} + \left[\Phi_2\right]\ddot{X}_{H2}\right)\right]$$

Insertion of the above equation into equations for X_{H1} and X_{H2} yields the following abbreviated equation set:

$$\left(\left[A22\right] + \left[\Phi_1\right]^T\left[U12\right]\left[\Phi_1\right]\right)\left\{\ddot{X}_{H1}\right\} + \left(\left[A23\right] + \left[\Phi_1\right]^T\left[U12\right]\left[\Phi_2\right]\right)\left\{\ddot{X}_{H2}\right\} = \left\{F_{H1} + \left[\Phi_1\right]^T V12\right\}$$

$$\left(\left[A23\right]^T + \left[\Phi_2\right]^T\left[U12\right]\left[\Phi_1\right]\right)\left\{\ddot{X}_{H1}\right\} + \left(\left[A33\right] + \left[\Phi_2\right]^T\left[U12\right]\left[\Phi_2\right]\right)\left\{\ddot{X}_{H2}\right\} = \left\{F_{H2} + \left[\Phi_2\right]^T V12\right\}$$

where

$$B12_M = kA12_M^T\, A11^{-1}$$

$$\left\{V12\right\} = \sum_{M=1}^{NB} B12_M\left\{F_{BM}\right\}$$

$$U12 = \sum_{M=1}^{NB} B12_M\, A12_M$$

Define

$$\left[B22\right] = \left[A22\right] + \left[\Phi_1\right]^T \left[U12\right]\left[\Phi_1\right]$$

$$\left[B23\right] = \left[A23\right] + \left[\Phi_1\right]^T \left[U12\right]\left[\Phi_2\right]$$

$$\left[B32\right] = \left[A23\right]^T + \left[\Phi_2\right]^T \left[U12\right]\left[\Phi_1\right]$$

$$\left[B33\right] = \left[A33\right] + \left[\Phi_2\right]^T \left[U12\right]\left[\Phi_2\right]$$

$$\left\{G1\right\} = \left\{F_{H1}\right\} + \left[\Phi_1\right]^T \left\{V12\right\}$$

$$\left\{G2\right\} = \left\{F_{H2}\right\} + \left[\Phi_2\right]^T \left\{V12\right\}$$

Then

$$\left\{\overset{**}{X}_{H2}\right\} = \left[B33\right]^{-1}\left\{\left\{G2\right\} - \left[B32\right]\left\{\overset{**}{X}_{H1}\right\}\right\}$$

Substitution yields

$$\left(\left[B_{22}\right] - \left[B23\right]\left[B33\right]^{-1}\left[B32\right]\right)\left\{\overset{**}{X}_{H1}\right\} = \left\{G1 - \left[B23\right]\left[B33\right]^{-1} G2\right\}$$

Solution of the equation above defines $\overset{**}{X}_{H1}$. Together with the equations for $\overset{**}{X}_{H2}$ and $\overset{**}{X}_{BM}$, the desired solutions are obtained.

4.1.8 Pitch-Gimbal Coupling

The pitch-gimbal coupling is the coupling between the individual blade pitch angles and the relative roll and pitch motions of the gimbal relative to the airframe. Figure 9 shows the gimbal roll, θ_{XG}, gimbal pitch, θ_{YG}, and blade azimuth angle location, Ψ. The other dimensions show the parameters identifying the pushrod location relative to the

blade. Given prelag angle, $-\delta_B$, and the location of the pushrod relative to the blade, Y_{10PR} and r_{5PR}, and the blade root attachment offset, e, the blade pitch change, $\Delta\theta$, can be calculated using the following equations:

$$\hat{\psi}_{PR} = \tan^{-1}\left(\frac{-e \sin\delta + Y_{10PR}}{r_{5PR}}\right)$$

$$\hat{r}_{PR} = \sqrt{\left(-e \sin\delta + Y_{10PR}\right)^2 + r^2_{5PR}}$$

$$\Delta\theta = \frac{r_{PR}}{Y_{10PR}}\left[\theta_{YG} \cos\left(\psi + \hat{\psi}_{PR}\right) - \theta_{XG} \sin\left(\psi + \hat{\psi}_{PR}\right)\right]$$

4.1.9 Ground Resonance Model

To analyze the ground resonance condition for an elastic gimbal rotor, it was necessary to add spring and damper characteristics representing the landing gear dynamics when the helicopter is on the ground. This requires, first of all, the determination of the force deflection characteristics at the hub in the hub coordinate system due to the presence of a spring and/or damper at a field point remote from the hub.

Referring to Figure 10 relate the field point to the untilted hub coordinate system (1):

$$\begin{Bmatrix} X \\ Y \\ Z \end{Bmatrix}_{FP} = \underbrace{\begin{bmatrix} 1 & 0 & 0 & -\Delta WL & 0 & -BL \\ 0 & 1 & \Delta WL & 0 & 0 & \Delta FS \\ 0 & 0 & BL & \Delta FS & 1 & 0 \end{bmatrix}}_{[T_1]} \begin{Bmatrix} X \\ Y \\ \theta_X \\ \theta_Y \\ Z \\ \theta_Z \end{Bmatrix}_{H1}$$

Relate untilted "1" coordinate system to tilted "2" coordinate system:

$$\begin{Bmatrix} X \\ Y \\ \theta_X \\ \theta_Y \\ Z \\ \theta_Z \end{Bmatrix}_{H1} = \underbrace{\begin{bmatrix} \cos\gamma_s & 0 & 0 & 0 & -\sin\gamma_s & 0 \\ 0 & 1 & 0 & 0 & 0 & 0 \\ 0 & 0 & \cos\gamma_s & 0 & 0 & -\sin\gamma_s \\ 0 & 0 & 0 & 1 & 0 & 0 \\ \sin\gamma_s & 0 & 0 & 0 & \cos\gamma_s & 0 \\ 0 & 0 & \sin\gamma_s & 0 & 0 & \cos\gamma_s \end{bmatrix}}_{[T_2]} \begin{Bmatrix} X \\ Y \\ \theta_X \\ \theta_Y \\ Z \\ \theta_Z \end{Bmatrix}_{H2}$$

Note: γ_s = rotor shaft tilt.

Field point elastic characteristics are then calculated as uncoupled spring-deflections:

$$\begin{Bmatrix} F_x \\ F_y \\ F_z \end{Bmatrix}_{FP} = - \underbrace{\begin{bmatrix} K_x & 0 & 0 \\ 0 & K_y & 0 \\ 0 & 0 & K_z \end{bmatrix}}_{[K]} \begin{Bmatrix} x \\ y \\ z \end{Bmatrix}_{FP}$$

Resolution of the resulting impedance characteristics at the hub then becomes:

$$\begin{Bmatrix} F_X \\ F_Y \\ \cdot \\ \cdot \\ M_Z \end{Bmatrix}_{H2} = \underbrace{-[T_2]^T [T_1]^T [K][T_1][T_2]}_{[TT]} \begin{Bmatrix} X \\ Y \\ \cdot \\ \cdot \\ \theta_Z \end{Bmatrix}_2$$

4.2 VALIDATION RESULTS

The validity of the computer analysis, G400, with the EGR modifications was established through a series of check cases with step-by-step buildup in the complexity of the math model; the results were examined for their reasonableness or compared to other analyses wherever possible.

4.2.1 Coupled Rotor/Gimbal System

The soft-inplane EGR configuration was first set up as a hingeless rotor with gimbal pitch and roll degrees of freedom. Figure 11 shows the time histories of the hub roll and pitch motions for fourteen rotor revolutions. The system is marginally stable with 1% blade lag damping and 1% gimbal damping. Frequencies for both the progressive lag mode, $\Omega + \omega_\zeta$, and the regressive lag mode, $\Omega - \omega_\zeta$, are evident in the time histories of the hub motion, with the latter being predominant.

With both lag damping and gimbal damping removed, Figure 12 shows that the system is slightly unstable. This is traced to the fact that the frequency of the rotor on the gimbal coupled with the rotor cyclic regressive flapping mode is in the proximity of the regressive lag mode. (A more detailed substantiation is discussed in the following subsection.) The stability characteristic exhibited is that of the classical ground resonance case. To illustrate this point, the configuration is analyzed with the gimbal stiffness arbitrarily increased from 90,133 ft-lb/rad to 499,008 ft-lb/rad and the damping in the lag mode and the gimbal removed. The resultant time histories in Figure 13 show that the system is stable even without any structural damping.

4.2.2 Coupled Rotor/Gimbal/Fuselage System

The preceding results are obtained without the airframe degrees of freedom. Figure 14 shows the time histories of the hub roll and pitch motion of the soft-inplane EGR coupled with the gimbal and the rigid airframe DOF in hover. There is a steady fall-off of the hub motion because the aircraft is unrestrained and is not precisely trimmed to maintain a zero mean position. Of significance is the oscillatory motion superimposed on the steady motion. The motion is slightly divergent at a frequency of 0.3P, the regressive lag mode frequency, with 1% damping in the blade and the gimbal.

Introduction of the rigid airframe DOF results in a slightly destabilized configuration. Figure 15 shows the hub motions of the coupled rotor and rigid-body airframe system without the gimbal. Using the same initial conditions as for the case shown in Figure 14 the coupled system is quite stable. Again the steady fall-off is due to a slightly out of trim condition. Note that the blade damping has been removed from the math model. A set of more severe initial conditions was imposed on this coupled rotor/airframe system in order to determine the dominant response frequency. Figure 16 shows that the resultant hub motions are responding in the air resonance mode at the regressive lag mode frequency of 0.3P. The motions, however, indicate that the coupled rotor and rigid-body airframe is stable even without the blade lag damping. These results demonstrate that the addition of the gimbal DOF causes the marginal stability of the EGR system. This is because the gimbal DOF, when coupled with the rotor regressive flap mode and the rigid airframe pitch and roll motions, introduces a coupled mode which is in the proximity of the regressive lag mode at the normal rotor speed.

Shown in Figure 17 as a function of the rotor speed are the coupled frequencies for a simplified math model of the EGR with the rigid airframe. Only two cyclic flapping degrees of freedom and the rigid airframe pitch and roll degrees of freedom are considered. The four resultant coupled modes are: the progressive flap mode, the cyclic flap/body roll mode, the cyclic flap/body pitch mode, and the rigid body pitch/roll mode, which lies on the abscissa and is therefore not shown. The two cyclic flap and rigid body pitch and roll modes are basically the regressive flap mode of the rotor coupled with the rigid airframe motions, with one being roll predominant and the other pitch predominant. The frequencies of these two modes are linear functions of the rotor speed because the equivalent springs for these modes are from the regressive flap mode whose frequency is dominated by the centrifugal force and therefore is proportional to the rotor speed. Also shown in Figure 17 are the regressive lag mode frequencies for the soft inplane rotor and for a stiff inplane configuration. At normal rotor speed, the cyclic flap/body roll mode and the cyclic flap/body pitch mode are well separated from the regressive lag mode of the soft inplane rotor. Consequently, there is no air resonance problem shown in Figure 16. The coupled rotor/rigid airframe system is stable.

Introducing the gimbal pitch and roll degrees of freedom alters the composition of the body modes. Analogous to a spinning top, the pitch and roll degrees of freedom of the gimbal are coupled by the rotating rotor and result in two modes: one at a frequency above 2P and the other at about zero frequency. When the gimbal springs are set to zero, the modal frequencies will be exactly 2P and zero. This lower-frequency mode of the gimbal couples with the rotor regressive flap mode and the airframe rigid pitch and roll degrees

of freedom to alter the composition of the body modes of interest. Figure 18 shows the coupled frequencies obtained with a math model consisting of six degrees of freedom: two cyclic flap, airframe rigid pitch and roll, and gimbal pitch and roll. The higher-frequency gimbal mode couples primarily with the rotor progressive flap mode, resulting in two coupled modes of very high frequency. These two frequencies are not shown in Figure 18. The lower-frequency gimbal mode, coupled with the rotor and the body, modifies the dynamic characteristics of the system in two significant ways, in addition to the obvious effect of introducing an extra mode. Comparing with Figure 17 in terms of the modal frequencies, these so-called "body modes" are relatively independent of the rotor speed variations. The coupled frequencies are determined now by the gimbal springs as well as the frequency of the regressive flap mode. This trend of frequency versus rotor speed as affected by the gimbal degrees of freedom is similar to that obtained from model tests (see Reference 4). The second effect is that, for the soft inplane EGR design, the gimbal degrees of freedom, when coupled with the regressive flap and airframe rigid pitch and roll, produce a coupled cyclic flap/body and gimbal roll mode which is in near resonance with the regressive lag mode at normal rotor speed. As shown in Figure 14, the resultant coupled rotor/gimbal/fuselage system is slightly unstable.

---

4. Bousman, W.G., AN EXPERIMENTAL INVESTIGATION OF THE EFFECTS OF AEROELASTIC COUPLINGS ON AEROMECHANICAL STABILITY OF A HINGELESS ROTOR HELICOPTER, Journal of the American Helicopter Society, Vol. 26, No. 1, January 1981.

4.2.3 Ground Resonance

To validate the G400 capability of calculating ground resonance, an articulated rotor configuration was set up on the G400 and the E927 computer programs. E927 is an eigensolution analysis. A rotor speed variation was conducted using E927 to obtain precise modal damping levels as a function of rotor speed. Two check cases, one stable (100% N_R) and the other unstable (124% N_R), were then run on G400. As shown in Figure 19, the damping levels from a log decrement calculation based on G400 time histories compare very well with the E927 eigensolutions. Actual G400 time histories are shown in Figure 20.

5.0 AEROELASTIC ANALYSIS

5.1 CHOICE OF BLADES AND BASELINE AIRCRAFT

The helicopter chosen for this study is a 10,000-lb gross weight aircraft with a four-bladed main rotor. The elastic gimbal rotor blades are based upon the articulated blades of this helicopter. The radius (22 ft), chord (1.3 ft), and tip speed (675 fpm) are the same. Weight and stiffness distribution outboard were kept approximately the same, but the articulated root was replaced with a flexible root end, with stiffness values chosen to provide two baseline blades: a soft inplane blade and a stiff inplane blade. The chordwise first mode natural frequency of the soft inplane blade is 0.72P and the natural frequency of the stiff inplane blade is 1.55P. The latter frequency was subsequently lowered to 1.3P for the baseline case. Figure 21 shows the effect of root end chordwise stiffness, EI, on the chordwise natural frequency. As shown, by varying EI out to 22% radius (0.22R) it was not possible to reach the chordwise natural frequency desired for the stiff blade. Therefore, for the stiff inplane blade, the chordwise EI was varied out to 0.4R. The analysis used to generate Figure 21 was approximate, and the natural frequencies generated for use in G400 differ slightly for a given stiffness, particularly for the stiff inplane rotor.

Flatwise stiffness was chosen to give a first flatwise frequency of 1.11P, and torsion was chosen to be at 5.9P. The blade configuration uses a torque tube and flexible beams to carry edgewise and flatwise loads. Therefore, the torsional stiffness is considered separately out to the attachment point to the blade at 0.22R. The blade properties are shown in Table 3 and in Figures 22 to 24. The blade mode shapes used in the G400 analysis are shown in Figures 25 to

Table 3.

ELASTIC GIMBAL ROTOR BLADE SECTION PROPERTIES

Coordinates are extremities of straight line segments which define the physical property curve.

WT/IN.		EI_f		EI_c Soft Inplane		EI_c Stiff Inplane
r/R	(LB/IN.)	r/R	(LB-IN.^{2}x10^6)	r/R	(LB-IN.^{2}x10^6)	
1.0	.1329	1.0	.628	1.0	37.4	
.953	.1329	.945	4.0	.95	198.5	
.953	.911	.945	5.3	.833	198.5	
.9303	.911	.833	5.3	.790	230.	
.9303	.3257	.795	5.72	.45	230.	
.7954	.3257	.700	5.72	.40	230.	840
.7954	.400	.682	5.40	.24	230.	|
.700	.400	.455	5.40	.24	300.	|
.700	.361	.398	5.96	.22	300.	|
.545	.361	.240	9.0	.22	40.	|
.545	.281	.240	25.	.12	40.	|
.240	.281	.220	25.	.08	200.	|
.240	1.15	.220	15.	.08	300.	|
.220	1.15	.12	15.	.0	300.	840
.220	.10	.08	30.			
.120	.10	.08	100.			
.080	.30	.06	100.			
.080	2.0	.06	50.			
.060	2.0	.02	50.			
.060	.50	.02	100.			
0.	.50	0.	100.			

Table 3. (continued)

GJ		I_p	
r/R	(LB-IN.^{2}x10^6)	r/R	(LB-IN.x10^6)
		1.0	3.74
1.0	7.0	.975	2.33
.947	7.0	.975	2.33
.45	7.0	.952	2.33
.24	12.50	.952	7.01
.24	20.	.923	7.01
.22	20.	.923	4.50
.22	.10	.795	5.26
.12	.10	.70	5.26
.08	5.0	.70	4.08
.08	50.	.24	4.08
.0	50.	.24	7.0
		.22	7.0
		.22	5.0
		.08	5.0
		0.	5.0

PITCH SHAFT PROPERTIES-GRAPHITE

r/R	WT/IN.	EI_f	EI_c	GJ	I_p
1.0	0.	0.	0.	0.	0.
.22	0.	0.	0.	0.	0.
.22	.25	3.8	3.8	12.	.2
.03	.25	3.8	3.8	12.	.2
.03	1.25	3.8	3.8	12.	35.
.02	1.25	3.8	3.8	12.	35.
.02	0.	0.	0.	0.	0.
0.	0.	0.	0.	0.	0.

27. These are cantilevered mode shapes. In the G400 analysis, these combine with the gimbal degree of freedom to provide the coupled system rotor modes.

5.2 AEROELASTIC STABILITY IN HOVER

The baseline EGR configuration was selected with the following pertinent features:

Flapwise frequency	1.11P
Edgewise frequency	1.30P
Edgewise damping	2% critical
Precone of pitch axis	2.5 deg.
Radial pitch link attachment point	12 in. from center
Chordwise pitch link attachment point	6.5 in. fwd.
Gimbal spring rate	195,000 ft-lb/rad
Gimbal damping	1% critical
Gimbal vertical offset from hub	4 in.

The choice of a stiff inplane rotor system requires some discussion. It is well known that the soft inplane hingeless rotor system with typical blade inplane frequency at 0.7P will have the potential of air resonance instability. This has been illustrated in Figure 17, which shows that the regressive lag mode corresponding to a soft inplane rotor is in close proximity to the cyclic flap/body roll mode at the normal rotor speed. The addition of the gimbal aggravates the situation by placing the coupled cyclic flap/body and gimbal roll mode in near resonance with the regressive lag mode at the normal rotor speed, as shown in Figure 18. In addition, the gimbal system also introduces an extra low frequency body mode which further restricts the placement of the operating rotor speeds. Similarly, the operating rotor speed will place a constraint on the freedom of selecting the gimbal springs. A stiff inplane rotor system, on the other hand, avoids the whole issue of air resonance. As shown in

Figure 18, although the frequency for the regressive lag mode corresponding to the 1.3P stiff inplane blade is almost identical to that of the soft case at normal rotor speed, due to the 180-degree phase shift from the soft to the stiff blade, the stiff inplane rotor will not encounter air resonance. There is, for the stiff inplane rotor, the issue of the coupled blade flap and lag instability (see Reference 5). This instability, however, is relatively mild and can be alleviated readily. For the gimballed rotor system, regardless of the inplane frequency there is an additional potential instability due to the coupled rotor and gimbal motion. This is discussed in the following paragraphs.

5.2.1 Mechanism for Coupled Rotor/Gimbal Stability

As depicted in Figure 28, when the blades are oscillating in the plane of rotation in a cyclic manner, centrifugal force imbalance is generated that causes the gimbal to tilt. As the blade pitch angle is coupled to the gimbal motion, there will be a cyclic pitch angle change due to the gimbal tilt. The resultant lift change will cause a cyclic flapping response which will be approximately 90 degrees away from the input cyclic pitch change, i.e., the gimbal tilt. A gyroscopic moment is generated by the cyclic flapping and is 90 degrees away from the flapping. Depending on the sense of the flapping, the resultant gyroscopic moment can be either in phase with the original gimbal tilt or out of phase with the tilt. Instability results in the former case, while the latter is stable.

---

5. Ormiston, R.A., and Hodges, D.H., FLAP-LAG DYNAMICS OF HINGELESS HELICOPTER ROTOR BLADES IN HOVER, Journal of the American Helicopter Society, Vol. 17, No. 2, April 1972.

The key to this potential instability is the blade pitch angle being coupled with the gimbal motion, or the so-called pitch-to-gimbal coupling described in Section 4.1.8. The sense of the coupling dictates the resulting flapping response, which in turn determines the direction of the gyroscopic moment and its effect of being stabilizing or destabilizing. A more thorough examination of the pitch-to-gimbal coupling is in order.

5.2.2 Pitch-to-Gimbal Coupling

The change in pitch angle due to the gimbal pitch and roll motions is expressed and shown in Section 4.1.8 as

$$\Delta\theta = \frac{\hat{r}_{PR}}{Y_{10PR}} \left[\theta_{YG} \cos\left(\psi + \hat{\psi}_{PR}\right) - \theta_{XG} \sin\left(\psi + \hat{\psi}_{PR}\right)\right]$$

In order to examine the relationship between θ and the gimbal motions θ_{XG} and θ_{YG}, let us simplify the expression by setting e = 0, i.e.,

$$\hat{r}_{PR} \sin \hat{\psi}_{PR} = Y_{PR}$$

$$\hat{r}_{PR} \cos \hat{\psi}_{PR} = r_{PR}$$

The change in pitch angle can now be simplified as

$$\Delta\theta = \left(\frac{r_{PR}}{Y_{PR}}\right)\left[\theta_{YG} \cos\psi - \theta_{XG} \sin\psi\right] - \left[\theta_{XG} \cos\psi + \theta_{YG} \sin\psi\right]$$

There are basically two parts to the pitch-to-gimbal coupling. The first part in the first bracket above depends on the radial and chordwise location of the pushrod attachment point to transfer the gimbal pitch and roll motion into blade

pitch angle change. Visualizing, for instance, a blade lined up with the downwind position, or $\Psi = 0$, when the gimbal is pitching with a magnitude of θ_{YG}, the pushrod attachment point, offset radially by r_{PR}, will have a vertical displacement of $r_{PR}\ \theta_{YG}$. Since the pushrod cannot deflect vertically or axially, and because it is offset in the chordwise direction by Y_{PR}, the blade will see a pitch angle change of $r_{PR}\theta_{YG}/Y_{PR}$. The second part of the pitch-to-gimbal coupling arises because of the relative motion between the swashplate and the gimbal, since the swashplate is fixed in space (to the airframe) during the gimbal excursion. Visualize again a blade lined up with the downwind position, when the gimbal is rolling with a magnitude of θ_{XG}. Since the swashplate remains horizontal, the entire relative motion θ_{XG} between the gimbal and the swashplate is transferred to the blade pitch independent of the pushrod location.

Two items of interest become evident. The first is that insofar as the swashplate does not follow the gimbal motion, there will always be pitch-to-gimbal coupling. The second is that changing the chordwise offset of the pushrod attachment point from the leading edge to trailing edge changes the sign of the part of the coupling that is dependent on the location of the attachment point. Also, the magnitude of the pitch-to-gimbal coupling depends on both the radial and chordwise offset distance. This fact can be used as a design parameter to vary the pitch-to-gimbal coupling readily.

5.2.3 Parametric Sensitivity

Five design parameters were investigated for their effect on the stability of the EGR: flap frequency, lag frequency, gimbal stiffness, gimbal height and pitch-to-gimbal coupling. The parameter variation is centered around the baseline value for a reasonable, practical range. Thorough investigation of

the parameter sensitivities is recognized to be useful but is beyond the scope of this contract.

Figure 29 shows the effect of the gimbal vertical height from the hub center and the pitch-to-gimbal coupling in terms of the radial distance of the pushrod attachment point. Varying the gimbal height from the baseline value of 4 inches, solid symbol, to a hub with the gimbal bearing at its center of rotation shows an improvement in the fixed system modal damping ratio. This is expected, since the less the vertical offset distance, the less the hub inplane translational motion due to the gimbal pitch and roll motions. This results in less excitation to the blade lag motion. As a consequence, the coupled rotor and gimbal system is more stable.

A desirable pushrod location is forward of the blade elastic axis. This is intended to introduce the conventional delta-3 coupling to alleviate the gust sensitivity for handling quality considerations. Holding the chordwise offset distance of 6.5 inches forward of the elastic axis as invariant, the radial offset distance has been varied from the baseline value of 12 inches to zero. As shown in Figure 29, the system stability is improved as the radial offset distance is decreased. This is precisely the effect of the pitch-to-gimbal coupling due to pushrod attachment geometry discussed earlier. Consider a blade at 90-degree azimuthal position. The blade will see an angle of attack decrease, with the leading edge horn arrangement, when the gimbal is tilting to the left. This coupling is reflected by the minus sign attached to the θ_{XG} term in the first bracket of the coupling equation. Losing lift at 90-degree azimuth, the blade will flap down in the front of the disc, or at 180 degree azimuth. The gyroscopic moment thus created will roll the disc toward

the left, aggravating the original gimbal left-roll excursion. Reducing this pitch-to-gimbal coupling by decreasing the radial offset distance of the pushrod is therefore stabilizing.

Increasing the gimbal stiffness from the baseline 195,000 ft-lb/rad is generally stabilizing, while the opposite is true for decreasing stiffness, as shown in Figure 30. Comparing the two dashed curves, triangles for the baseline inplane frequency of 1.3P and circles for inplane frequency of 1.55P, the higher inplane frequency results in a less stable system for the range of gimbal stiffness investigated. Of interest is the third curve in Figure 30, with the square symbols. This curve is calculated with an inplane frequency of 1.55P, the same as the dashed curve with the circles. Instead of the baseline pushrod location, the pushrod has been moved to the trailing edge with zero radial offset. With the pushrod-location dependent pitch-to-gimbal coupling removed, the system is a good deal more stable than the one with the baseline pushrod location.

Figure 31 shows the effects of the inplane frequency and the flap frequency on the system stability. While the stability improves as the lag frequency is reduced from 1.55P to 1.3P to 1.15P, the stability deteriorates when the flap frequency is decreased from 1.2P to 1.11P to 1.05P. The lag frequency effect is most likely due to the fact that the regressive lag mode frequency is approaching zero as the lag frequency is decreased toward 1P; consequently, it requires less damping to stabilize the system. As for the trend with the flap

frequency, the available roll damping of the gimbal is directly proportional to the flap frequency (see Reference 6). Reducing flap frequency decreases the available damping and results in a less stable system.

A soft inplane EGR has also been evaluated. Although, in addition to the potential stability problem faced by the stiff EGR, it also has the potential air resonance problem, the soft design was found to be stable with 5% inplane damping. Since this damping value was greater than that required for the stiff inplane rotor, the stiff rotor was chosen for the parametric study.

5.3 AEROELASTIC STABILITY ON THE GROUND

The model used to analyze the aeroelastic stability characteristics of the EGR on the ground is basically the same one used in hover, i.e., rotor on gimbal that is supported by the airframe rigid body DOF. Ground springs were used to constrain the rigid airframe DOF. These ground springs were determined by using a typical landing gear package which includes the oleo and the tires for a 10,000-pound helicopter.

For the ground stability calculations, two parametric values were changed from the baseline values defined in Section 5.2. The gimbal stiffness was decreased to 90,133 ft-lb/rad because it provides a more suitable hub moment characteristic. Since the lowered gimbal stiffness results in a less stable system, using this gimbal stiffness is a conservative approach. The radial offset of the pushrod location was

---

6. Burkam, J.E., Miao, W., EXPLORATION OF AEROELASTIC STABILITY BOUNDARIES WITH A SOFT-IN-PLANE HINGELESS ROTOR MODEL, Journal of the American Helicopter Society. Vol. 17, No.4, October 1972.

moved inboard from 12 inches to 3 inches. This is a more desirable location from the design arrangement point of view, and as shown in Figure 29, it is also beneficial from the system stability point of view.

Figure 32 shows that the baseline stiff inplane EGR system is quite stable at normal rotor speed during takeoff, with the blade inplane damping assumed to be 2% critical. At zero percent airborne, the system is most stable with 19% modal damping. A slight drop-off in modal damping accompanies increasing percent airborne until at 100% airborne, or in hover, the modal damping reaches a low of 17.5% critical.

Also shown in Figure 32 is the ground stability of a soft inplane EGR. The system is stable with 3% critical modal damping and 5% blade inplane damping. The drop off in stability from the stiff inplane configuration to the soft inplane case is because the latter configuration is susceptible to the ground resonance phenomenon. Some blade inplane damping is necessary to stabilize the system.

5.4 FORWARD FLIGHT ANALYSIS

A limited evaluation of the EGR in forward flight was conducted. Level flight at 145 knots at 10,000-lb gross weight was considered. The capability of the G400 analysis to provide trimmed flight conditions limited the usefulness of the program for forward flight evaluation. More program development is needed to provide automated trim conditions in the G400 analysis to speed the conversion of the program to the described flight condition. This is particularly needed for complex configurations such as the EGR, which involve separate rotor, hub, and airframe degrees of freedom.

To expedite the trimming of a gimbal rotor, the procedure used was to trim a rotor to near-zero 1P flapping at the required lift and propulsive force with the gimbal degrees of freedom locked out. This simulates the response of an EGR. Figure 33 shows the results of this approach for the stiff inplane rotor. With the gimbal locked out it is acting as a bearingless rotor. It was then planned to rerun the case using the trimmed conditions for the gimbal-locked case as the initial conditions for the gimbal-freed case, including using the shaft inclination angle as the initial condition for the gimbal tilt angle. Repeated attempts at running the gimbal-freed case gave inconsistent trends for the relationships between cyclic pitch, aerodynamic rotor moment, gimbal tilt angle, and blade tip path plane angle. More work is needed to examine the G400 analysis for use as a forward flight analysis for an EGR configuration. Testing of an EGR model is also needed to provide data for correlation with the analysis. Until this is done, the results of the analysis for forward flight cases cannot be relied upon.

5.5 CORIOLIS ACCELERATION EFFECTS

The cases run do indicate the effectiveness of the EGR in reducing Coriolis forces. The Coriolis acceleration contributes significantly to the edgewise bending moments on a blade with no lag hinge. The principal component is a 1P moment. This results primarily from the 1P flatwise bending of the blade. This component of Coriolis acceleration is proportional to the product of the rotor rotational speed, the steady flatwise bending displacement, and the 1P flatwise bending velocity. The Coriolis acceleration results from the requirement of the blade dynamics to change the inplane linear velocity of a blade element (caused by rotational speed) as the blade element moves radially inward or outward. Flapping about a coned position creates such radial motion of

a blade element. If the blade has a lag hinge, the result of the 1P Coriolis acceleration is a 1P lag motion. A blade without a lag hinge reacts the Coriolis acceleration forces by bending in the inplane direction with 1P bending moments in the blade.

The EGR reduces the Coriolis effects on bending by reducing the 1P flatwise bending of the blade. Figure 33 shows results from a G400 analysis of two rotors in forward flight. Both have the same lift and propulsive force and the same flight speed of 145 knots. The top rotor is a hingeless rotor in which flatwise bending of 3 degrees is required to provide the propulsive force. Note that the edgewise tip deflection is about 12 inches peak-to-peak. The rotor in the lower half of the figure simulates an EGR. It has very little 1P flatwise deflection. The corresponding edgewise peak-to-peak tip deflection is less than 6 inches. The analysis indicates a similar drop in edgewise vibratory bending moment at the root of the blade. The Coriolis effects are the predominant reason for the difference, as the rotor attitude relative to the airstream is very similar for the two rotors. By reducing the 1P flatwise deflection, the Coriolis force effects are significantly reduced.

6.0 DISCUSSION OF RESULTS

The results of this preliminary study support the feasibility of the elastic gimbal rotor. From the evaluation of the structural loads it is evident that the gimbal spring is the critical component in the rotor system, and careful attention must be paid to its design to provide both adequate fatigue strength and the stiffness required for the desired level of control power. The design of the blade torsionally flexible beams will also require extensive analysis, particularly if the twin beam design is used. Practical designs for all EGR components should be achievable, however. The EGR concept is feasible based on structural loads requirements.

The aeroelastic analysis of the EGR using G400 has also shown that the rotor concept is feasible. This was a preliminary study, and considerable time was required to modify the analysis to model the EGR. Additional time was required to understand the implications of the EGR response calculated by the G400 analysis, as the rotor has characteristics which make it different from other rotor systems. The pitch-to-gimbal coupling involving the swashplate fixed to the airframe and affecting pitch through gimbal motion and the coupling of the gimbal spring with the blade modes are particularly significant. Further analysis is needed to evaluate the many design parameters which could affect the response of the EGR and to determine what their effects are so that the best combination of parameters can be incorporated.

It has been learned that a stable EGR configuration having a suitable gimbal stiffness for control power requirements can be defined. The trends of many of the key variables on hover stability were defined and will be useful in further design work. The analysis has indicated that either a stiff inplane

rotor or a soft inplane rotor can be used. Augmented structural damping may be needed for the soft inplane rotor. Further design analyses to establish the structural properties of a dual flexible beam blade to meet the blade inplane frequency requirements must be carried out. More sophisticated analysis and confirming tests will be required.

The location of the pitch horn is an interesting aspect of the design. A leading edge horn was found to be acceptable. This location is preferable from an overall design integration requirement. Many rotors using gimbal joints,such as the McDonnell XV-1, the Bell tilt rotor, and the Doman rotor, have had trailing horns. The reasons for this choice apparently were different in each case, however, and are not directly pertinent to the EGR requirements. The McDonnell rotor uses a trailing horn to provide pitch-flap (δ_3) coupling for their blade which has an offset flap hinge (see Reference 7). The use of the trailing edge horn permits the push-rods to be grouped near the rotor shaft. Bell reported (Reference 8) that negative δ_3 provided better response characteristics for a tilt rotor in the propeller mode. Therefore, a trailing horn would be beneficial. Neither reason dictates a need for a trailing horn on the EGR.

---

7. Hohenemser, K.H., and Perisho, C.H., ANALYSIS OF THE VERTICAL FLIGHT DYNAMIC CHARACTERISTICS OF THE LIFTING ROTOR WITH FLOATING HUB AND OFF-SET CONING HINGES, Journal of the American Helicopter Society, Volume 3, No. 4, October 1958.
8. Gaffey, T., THE EFFECT OF POSITIVE PITCH-FLAP COUPLING (NEGATIVE $_3$) ON ROTOR BLADE MOTION STABILITY AND FLAPPING, Journal of the American Helicopter Society, Vol. 14, No. 2, April 1969.

Experimental confirmation of the elastic gimbal rotor by dynamically scaled model tests is also recommended for the evaluation of the concept. This will confirm the feasibility of the concept and will provide data for correlation of the G400 analysis. The latter is very important, for the EGR is sufficiently different from other rotors that our experience using G400 to analyze other rotors cannot be relied upon to establish our confidence level in the EGR results. At this point the EGR concept continues to look promising, but more work must be done. This study was very valuable in furthering the understanding of the EGR and in providing a better analytical capability to evaluate it.

7.0 CONCLUSIONS

1. Based on this preliminary study, the elastic gimbal rotor is feasible, and development of it should continue.

2. Either a stiff inplane or a soft inplane rotor blade may be used, although higher edgewise blade damping appears to be required with a soft inplane blade.

3. Practical designs for all EGR components should be achievable to satisfy structural loads requirements.

4. The EGR was found to be stable on the ground and in hover.

5. Forward flight analysis was not sufficient to define stability characteristics and stress limits, and further analysis should be conducted.

6. The stability margin was found to be sensitive to a number of design parameters, and additional studies of other design parameters should be conducted.

8.0 RECOMMENDATIONS

1. Continue development of the EGR concept through continued analytical and design studies.

2. Conduct model tests of the EGR on a hover stand and in a wind tunnel to confirm concept feasibility and design requirements and to correlate with analysis.

REFERENCES

1. Dixon, P. G. C., DESIGN, DEVELOPMENT, AND FLIGHT TEST DEMONSTRATION OF THE LOADS AND STABILITY CHARACTERISTICS OF A BEARINGLESS MAIN ROTOR, Boeing Vertol Company, USAAVRADCOM-TR-80-D-3, Applied Technology Laboratory, U.S. Army Research and Technology Laboratories, Fort Eustis, Virginia, June 1980, AD A086754.

2. Bielawa, R.L., AEROELASTIC ANALYSIS FOR HELICOPTER ROTOR BLADES WITH TIME-VARIABLE NONLINEAR STRUCTURAL TWIST AND MULTIPLE STRUCTURAL REDUNDANCY - MATHEMATICAL DERIVATION AND PROGRAM USER's MANUAL, United Technologies Research Center, NASA Contractor Report CR-2638, Langley Research Center, National Aeronautics and Space Administration, Langley, Virginia, October 1976.

3. Houbolt, J.C., and Brooks, G.W., DIFFERENTIAL EQUATION OF MOTION FOR COMBINED FLAPWISE BENDING, CHORDWISE BENDING, AND TORSION OF TWISTED NON-UNIFORM ROTOR BLADES, NACA Report 1346, 1958.

4. Bousman, W. G., AN EXPERIMENTAL INVESTIGATION OF THE EFFECTS OF AEROELASTIC COUPLINGS ON AEROMECHANICAL STABILITY OF A HINGELESS ROTOR HELICOPTER, Journal of the American Helicopter Society, Vol. 26, No. 1, January 1981.

5. Ormiston, R.A., and Hodges, D. H.,FLAP-LAG DYNAMICS OF HINGELESS HELICOPTER ROTOR BLADES IN HOVER, Journal of the American Helicopter Society, Vol. 17, No. 2, April 1972.

6. Burkam, J. E. and Miao, W., EXPLORATION OF AEROELASTIC STABILITY BOUNDARIES WITH A SOFT-IN-PLANE HINGELESS ROTOR MODEL, Journal of the American Helicopter Society, Vol. 17, No. 4, October 1972.

7. Hohenemser, K.H., and Perisho, C.H., ANALYSIS OF THE VERTICAL FLIGHT DYNAMIC CHARACTERISTICS OF THE LIFTING ROTOR WITH FLOATING HUB AND OFF-SET CONING HINGES, Journal of the American Helicopter Society, Vol. 3, No. 4, October 1958.

8. Gaffey, T., THE EFFECT OF POSITIVE PITCH-FLAP COUPLING (NEGATIVE δ_3) ON ROTOR BLADE MOTION STABILITY AND FLAPPING, Journal of the American Helicopter Society, Vol. 14, No. 2, April 1969.

LIST OF SYMBOLS

a_{1s} - Cosine component of first harmonic flapping

b - Number of blades

c - Distance to outer fiber of section

E - Modulus of elasticity

e - Flap hinge offset

e_{eq} - Equivalent hinge offset

F - Force

F_c - Centrifugal force

G - Torsional modulus

I - Moment of inertia

I_c - Chordwise moment of inertia

I_f - Flatwise moment of inertia

I_p - Polar moment of inertia

J - Torsional moment of inertia

K - Spring rate and hub moment constant

L - Length

LIST OF SYMBOLS (Continued)

M - Moment

$\bar{m}$ - Mass per unit length

M_i - Generalized mass

M_o - Reference mass per unit length

NB - Number of blades

Q - Torque

R - Blade radius

R_H - Radius to gimbal spring attachment

r - Radius

S - Stress

t - Thickness

V - Shear force

W - Blade vertical deflection

x - Radial displacement

y - Inplane displacement

z - Vertical displacement

γ_H - Gimbal tilt angle

γ_{TPP} - Tip path plane angle

ε - Strain rate

θ_x - Roll angle

θ_y - Pitch angle

θ_z - Yaw angle

ρ - Radius of curvature

ρ - Air density

σ - Rotor solidity

τ_s - Steady shear stress

τ_v - Vibratory shear stress

Ψ - Blade azimuth angle

Ω - Rotational speed

ω_ζ - Blade edgewise natural frequency

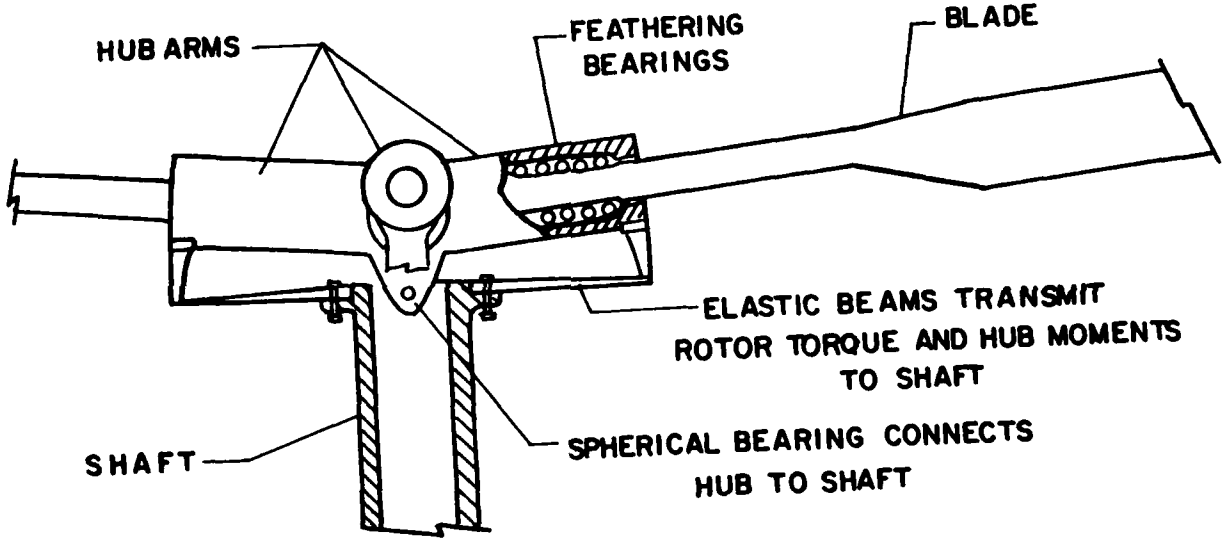

Figure 1. Schematic Arrangement of the Elastic Gimbal Rotor.

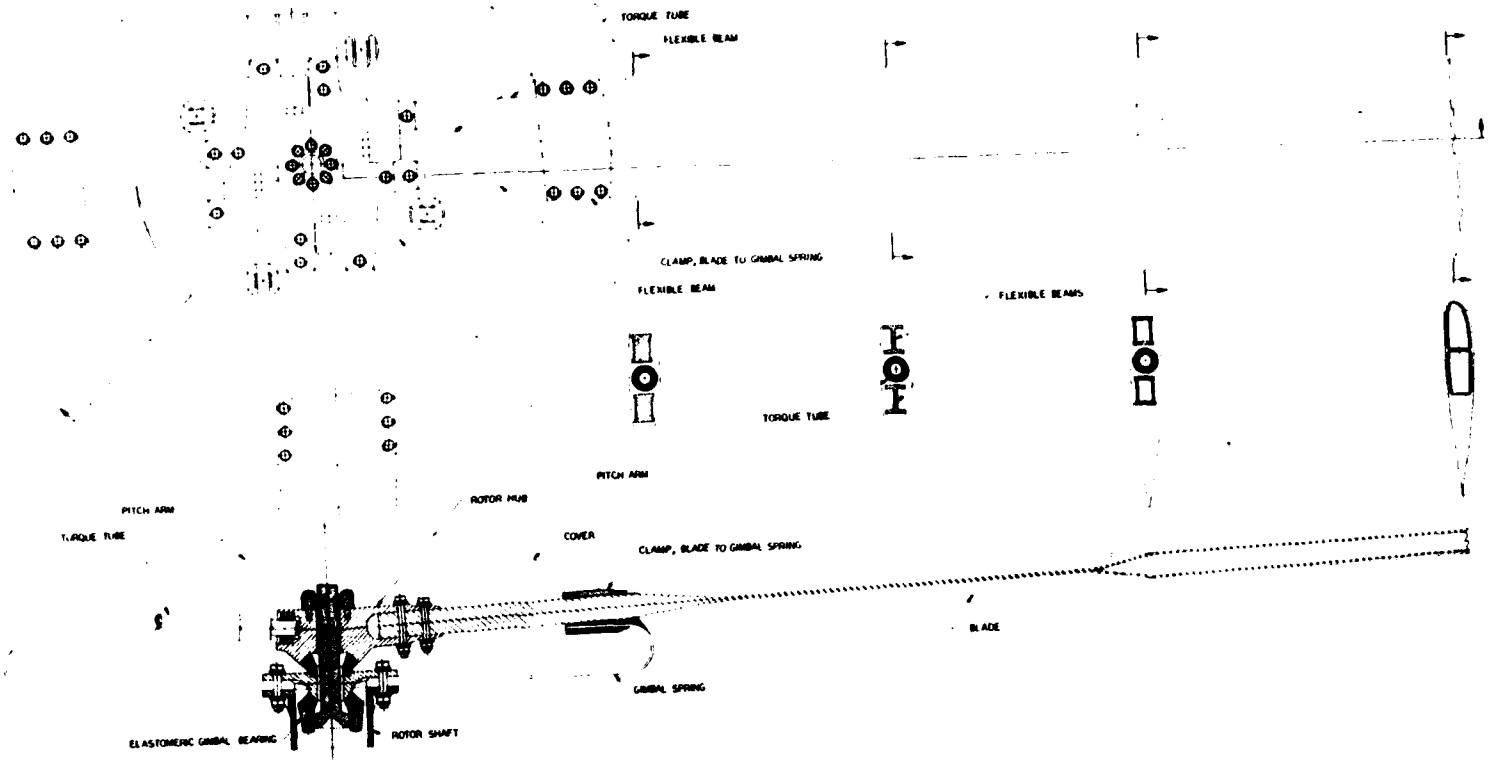

Figure 2. Elastic Gimbal Rotor Design.

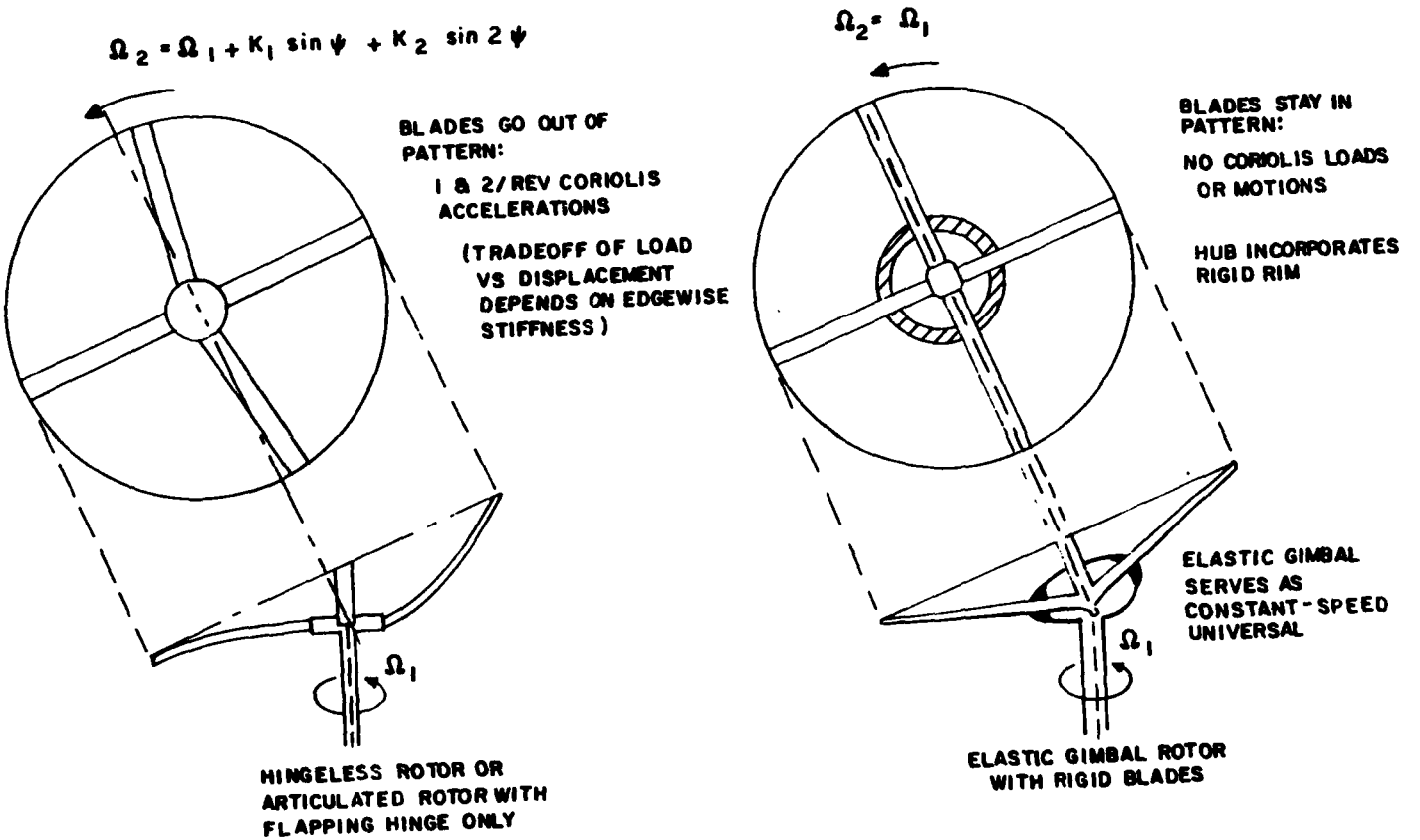

Figure 3. Coriolis Effects Suppressed in Elastic Gimbal Rotor.

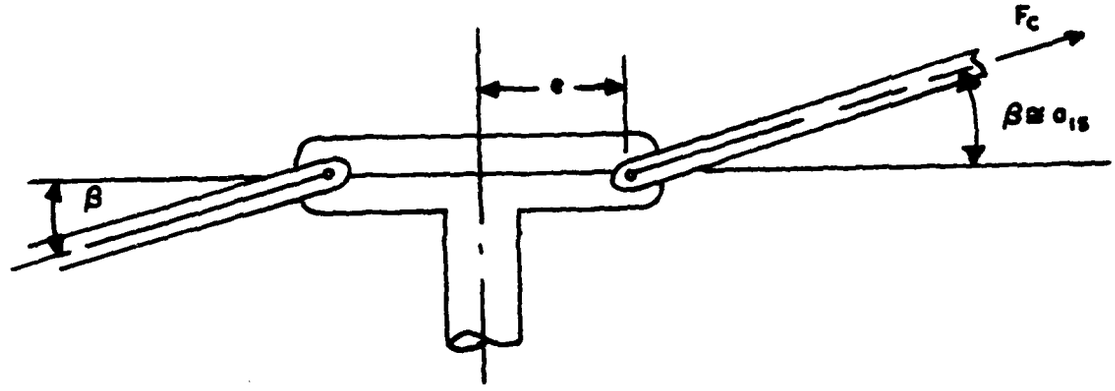

ARTICULATED ROTOR

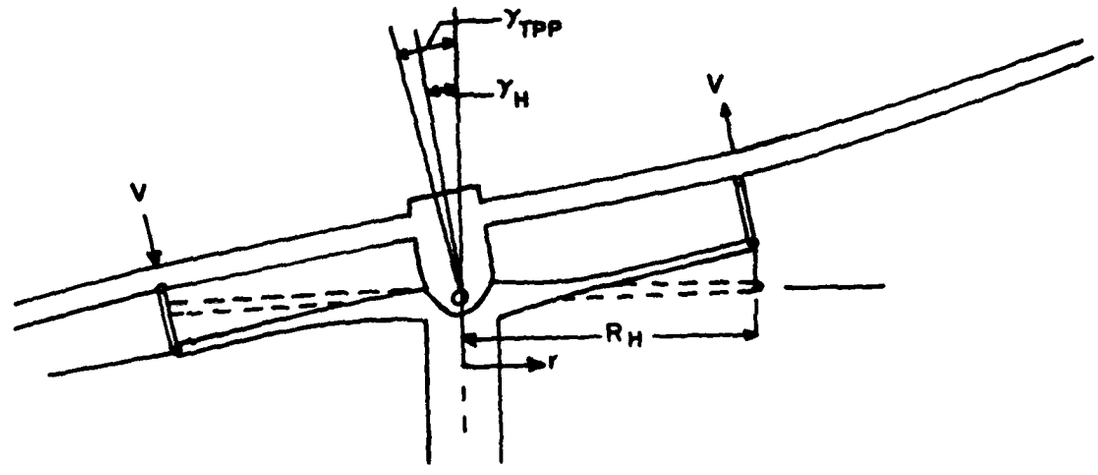

ELASTIC GIMBAL ROTOR

Figure 4. Hub Moments for an Articulated Rotor and an EGR.

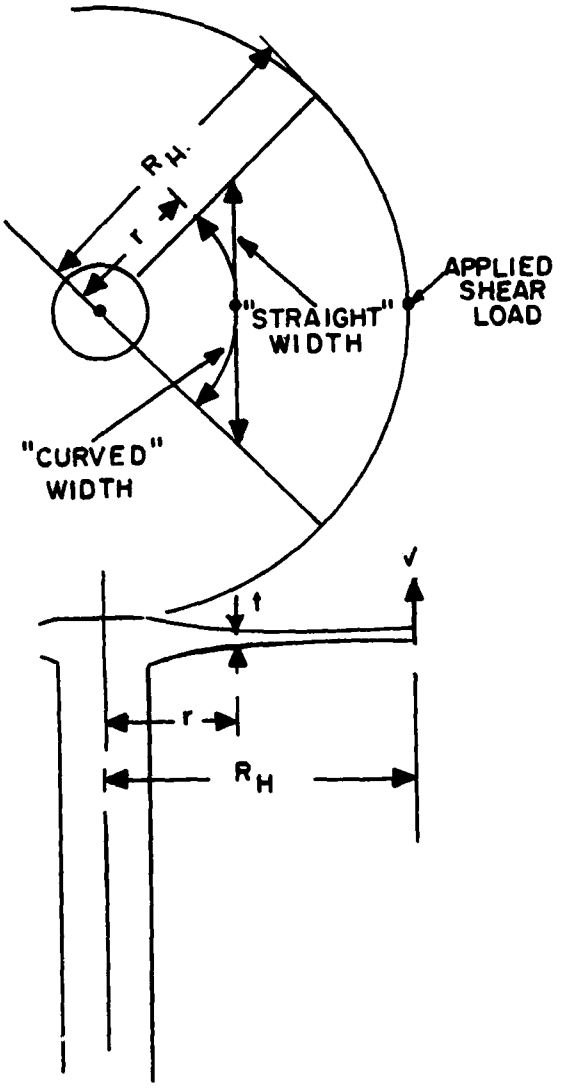

Figure 5. Gimbal Spring Stiffness Model.

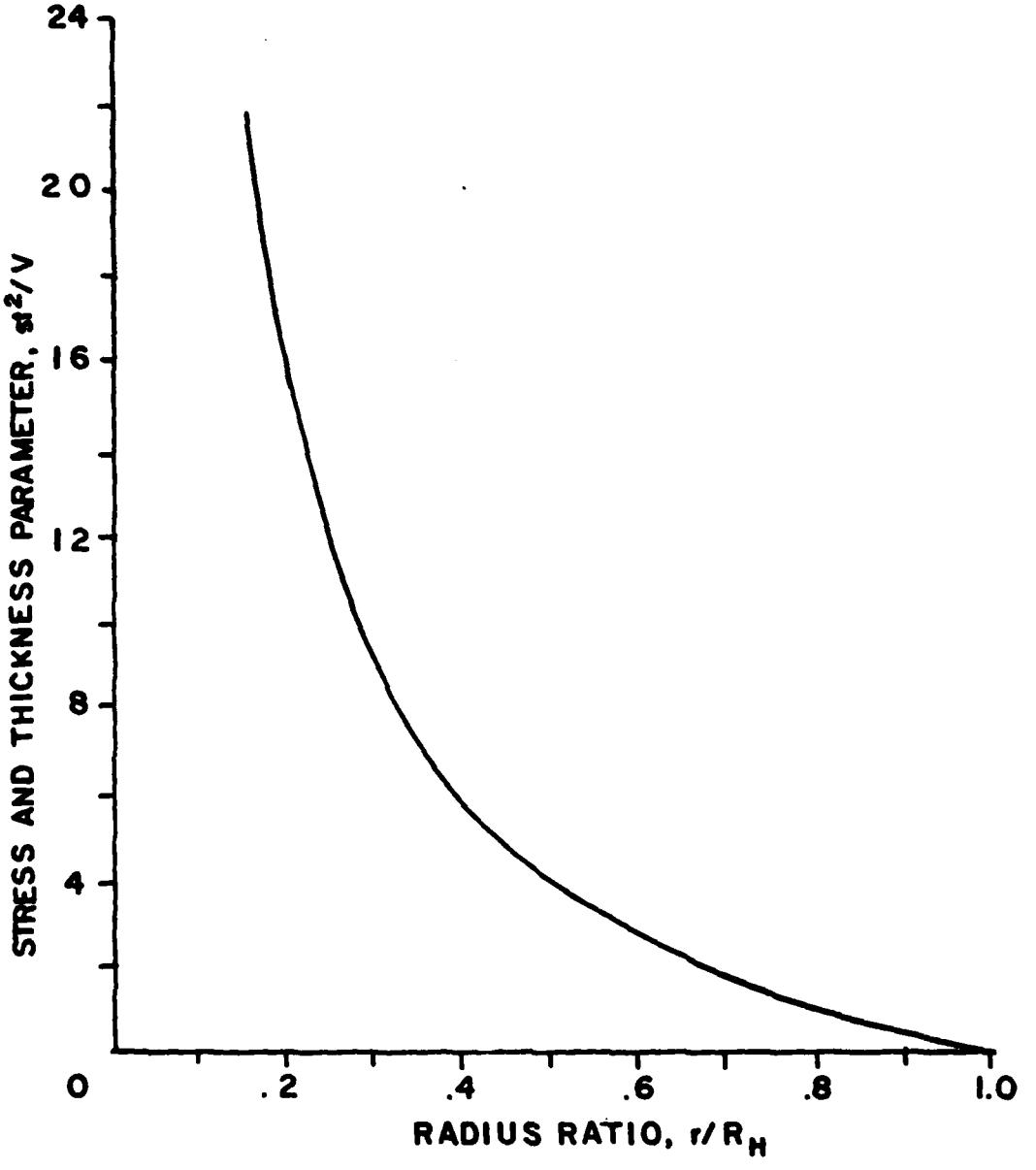

Figure 6. Stress and Thickness Parameter.

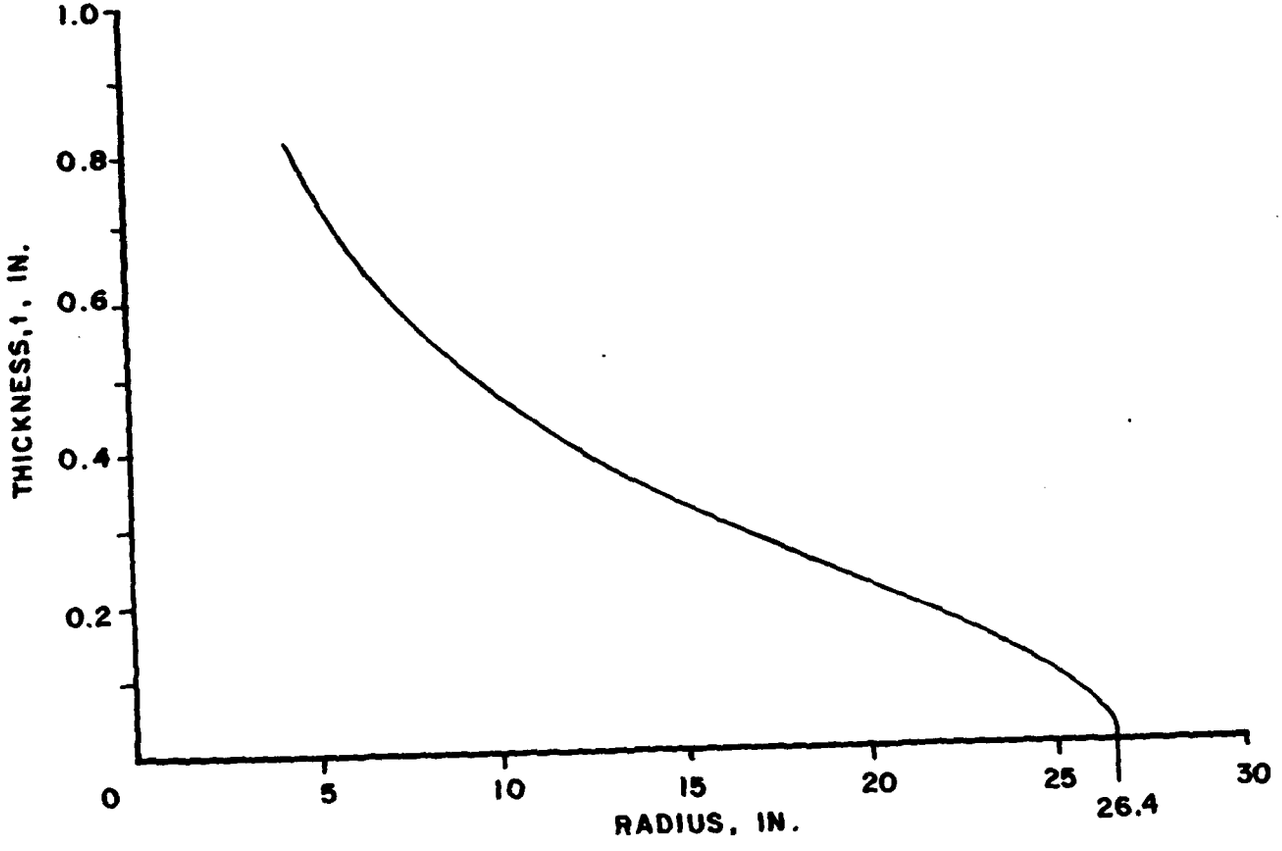

Figure 7. Gimbal Spring Thickness Distribution for Constant Bending Stress of 40,000 psi.

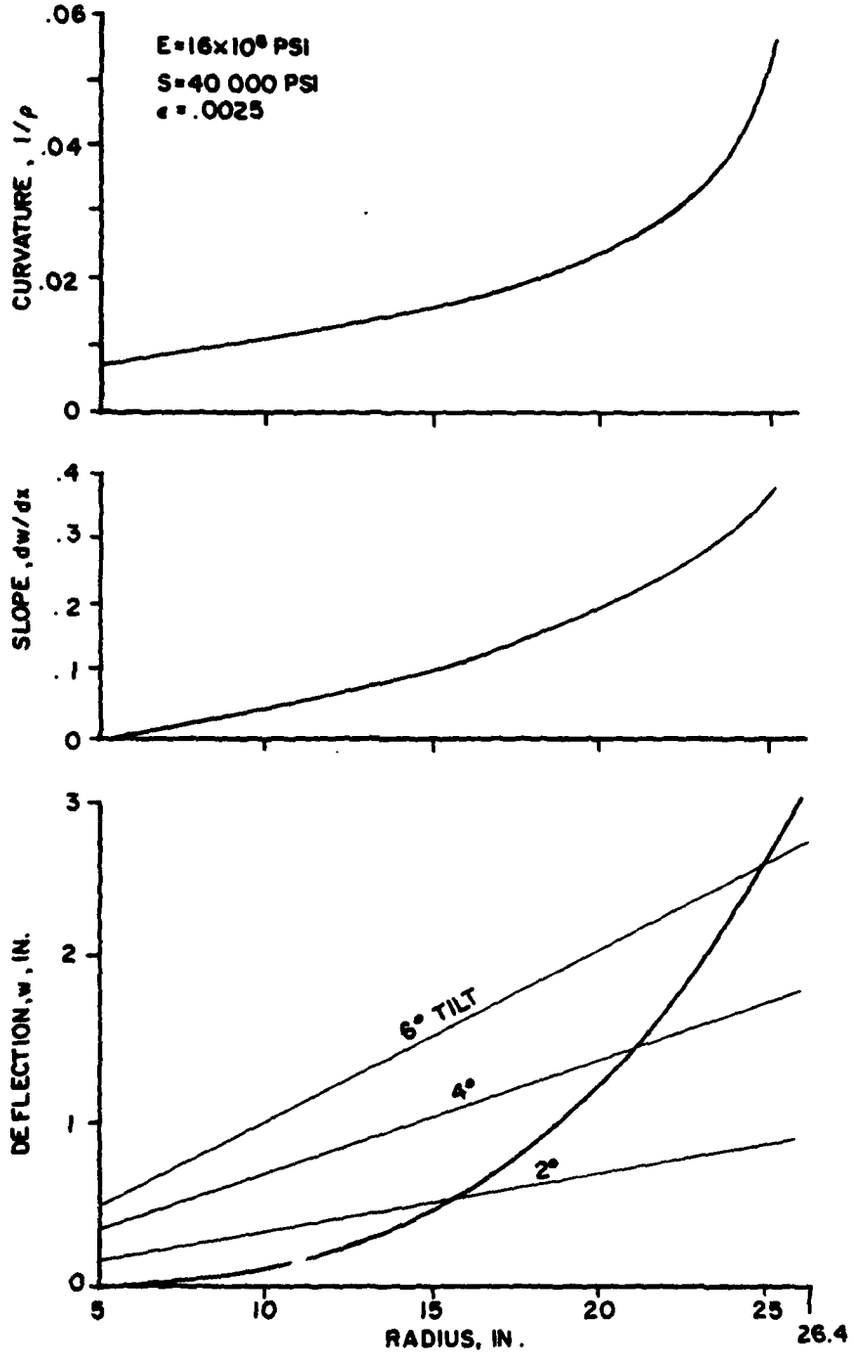

Figure 8. Curvature, Slope and Deflection of Gimbal Spring.

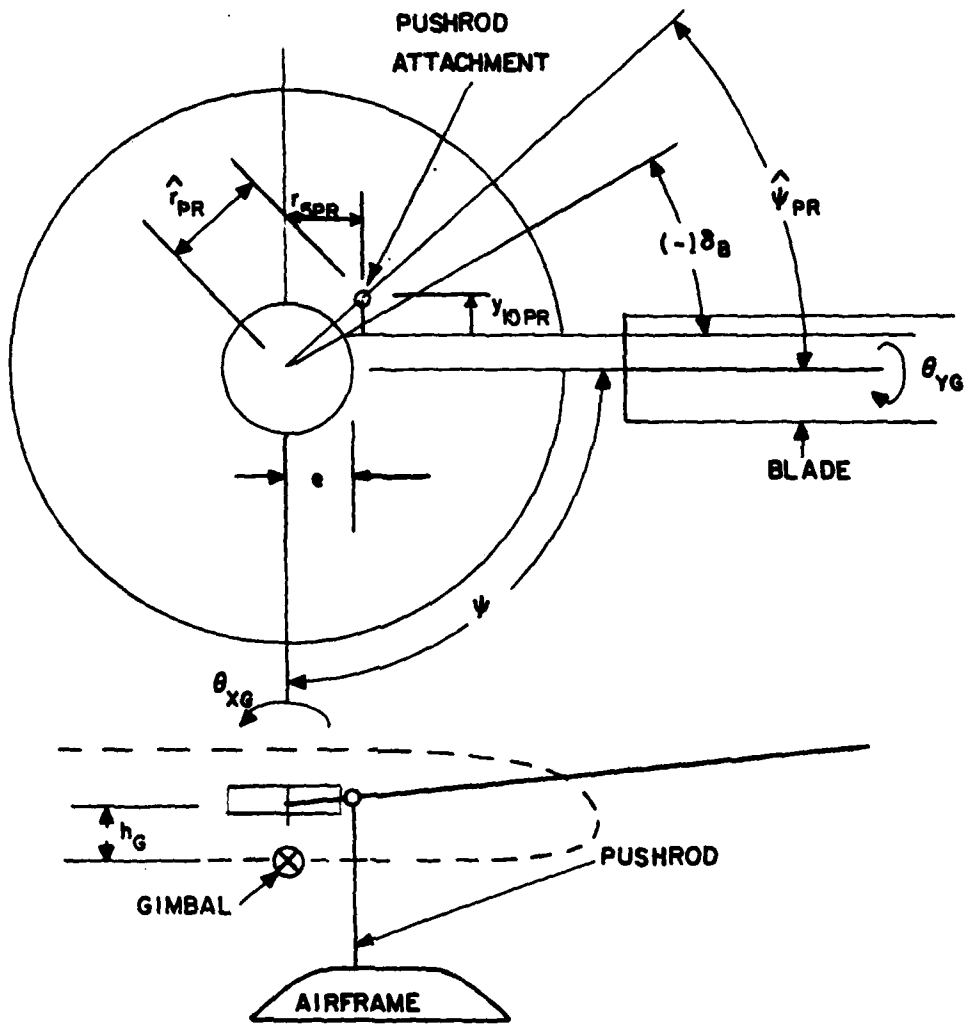

Figure 9. Pitch-Hub Tilt Coupling.

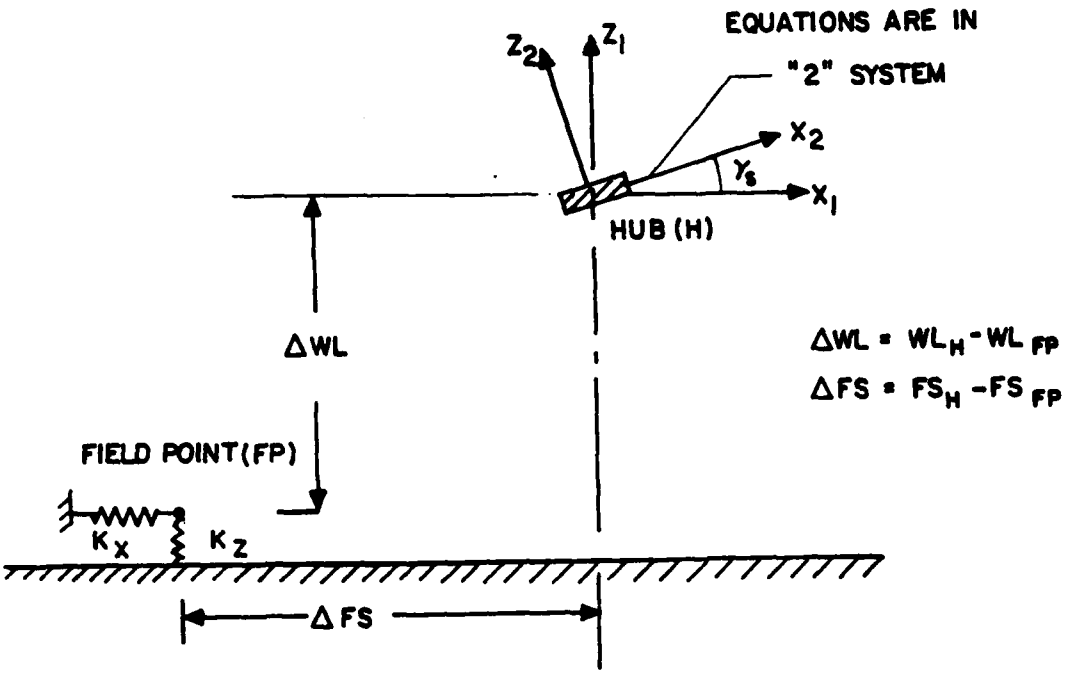

Figure 10. Coordinate Transformations for Ground Resonance Model.

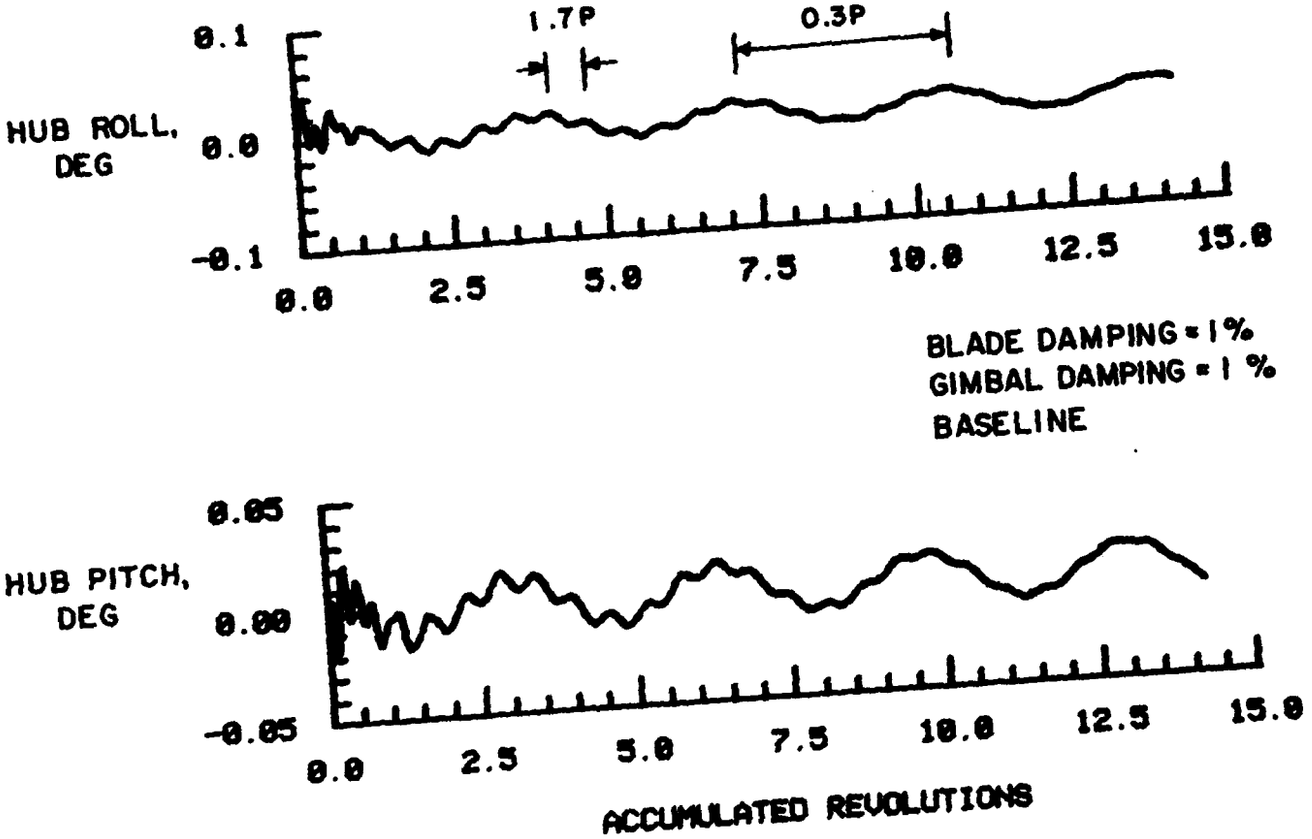

Figure 11. Soft Inplane Blade Stable in Hover.

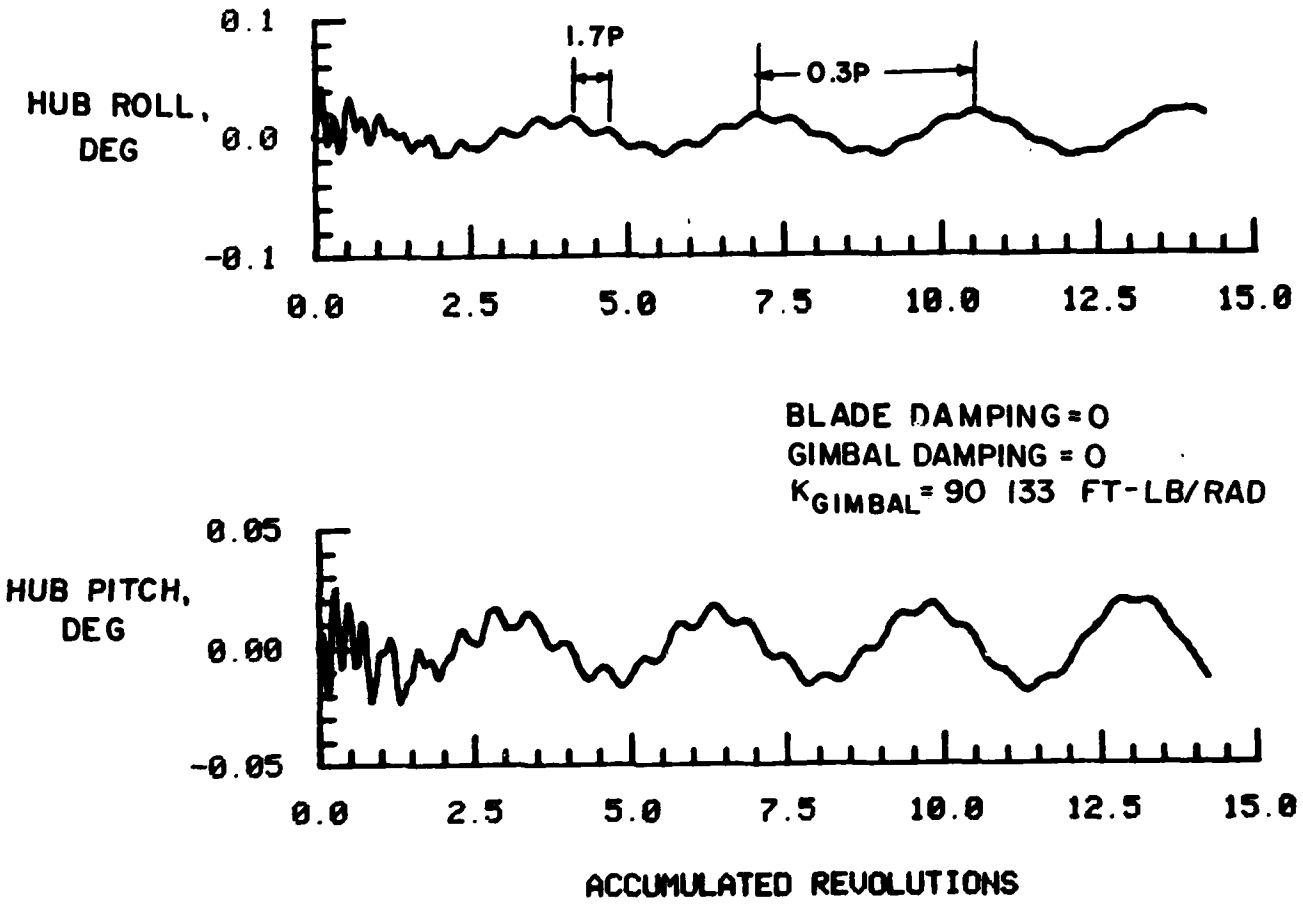

Figure 12. Removing Structural Damping Destabilizes Rotor

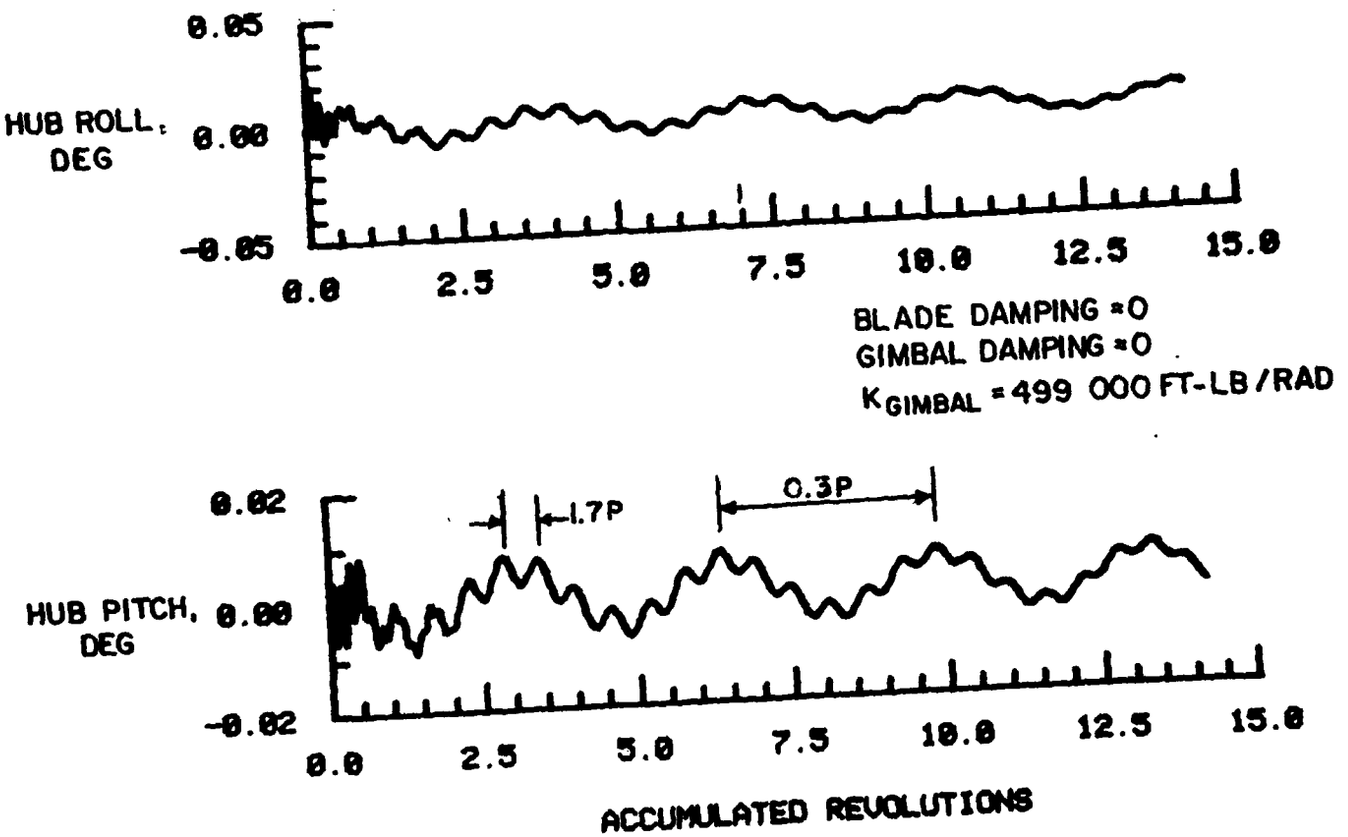

Figure 13. Increasing Hub Stiffness Stabilizes Rotor

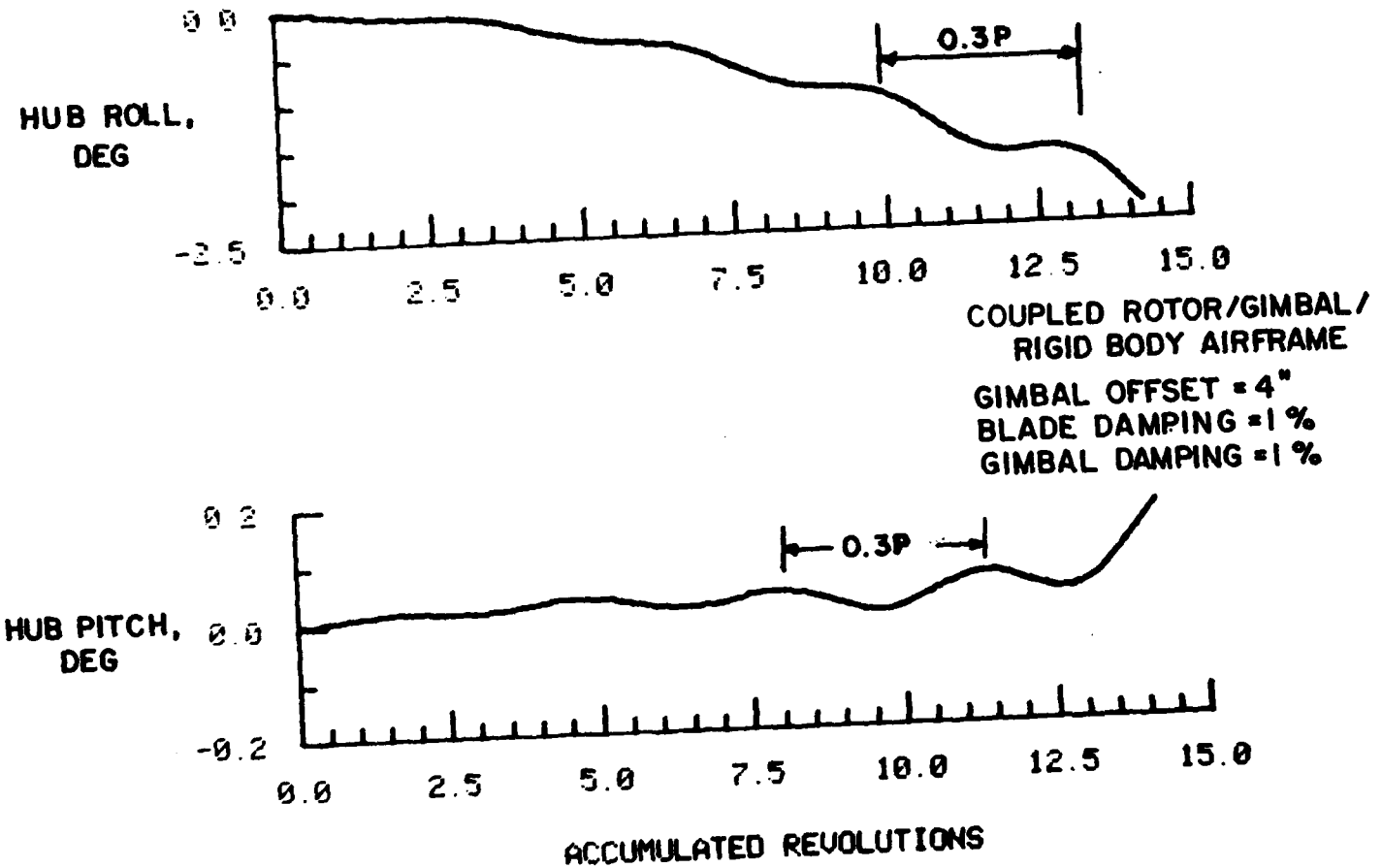

Figure 14. Addition of Airframe (Rigid Body) Destabilizes System

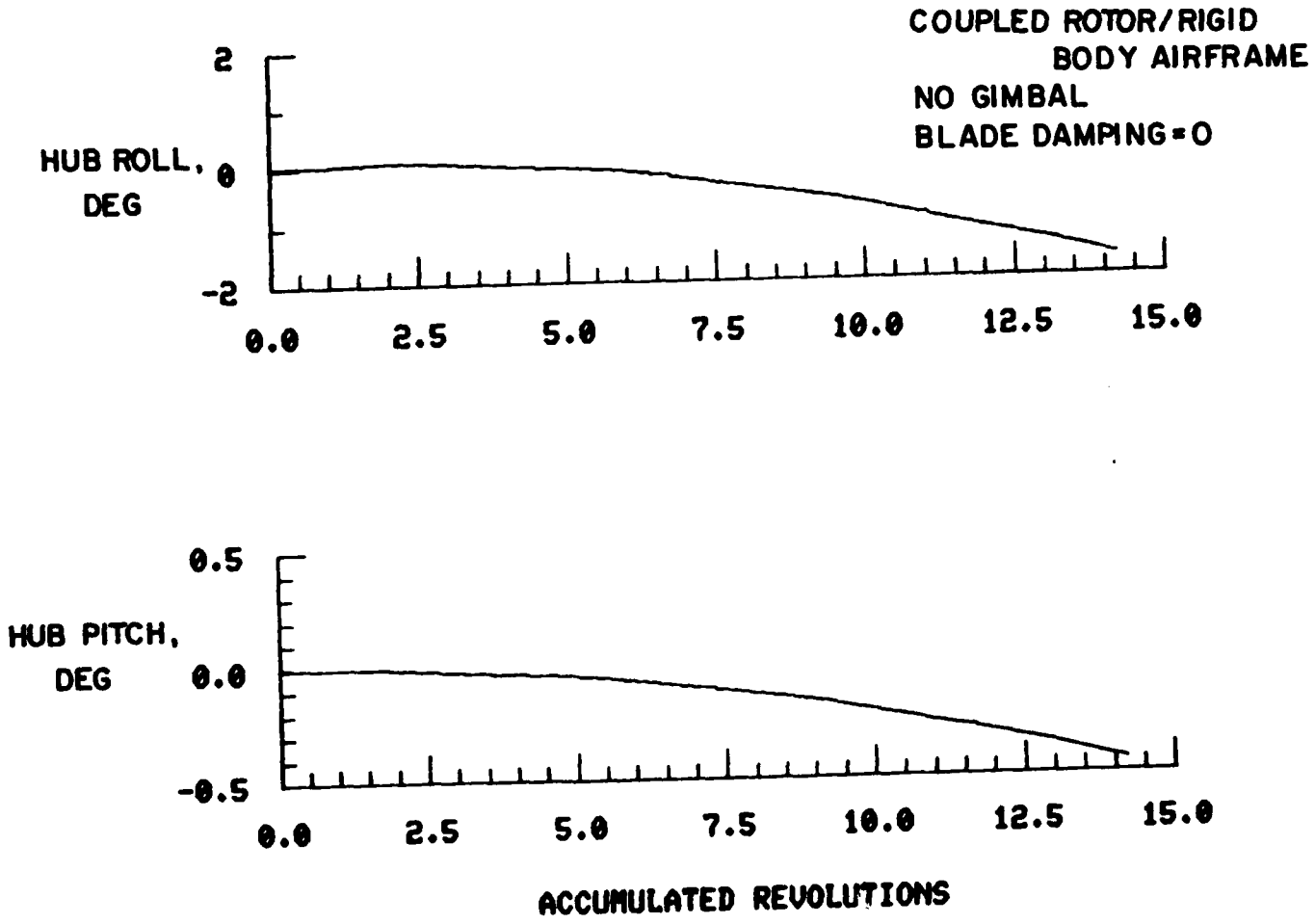

Figure 15. Removal of Gimbal DOF Stabilizes Rotor

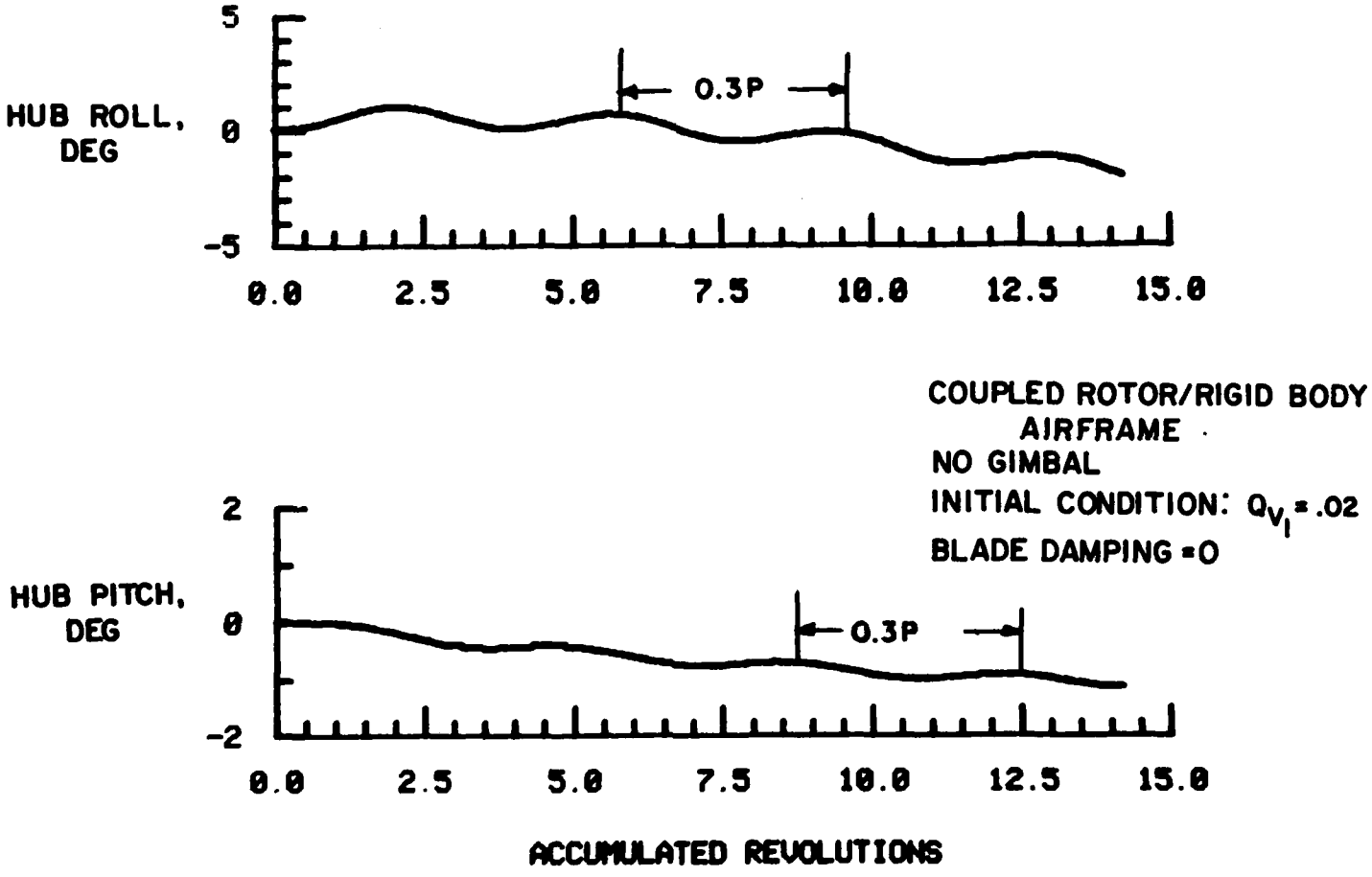

Figure 16. Rotor Without Gimbal with Larger Initial Blade Displacement.

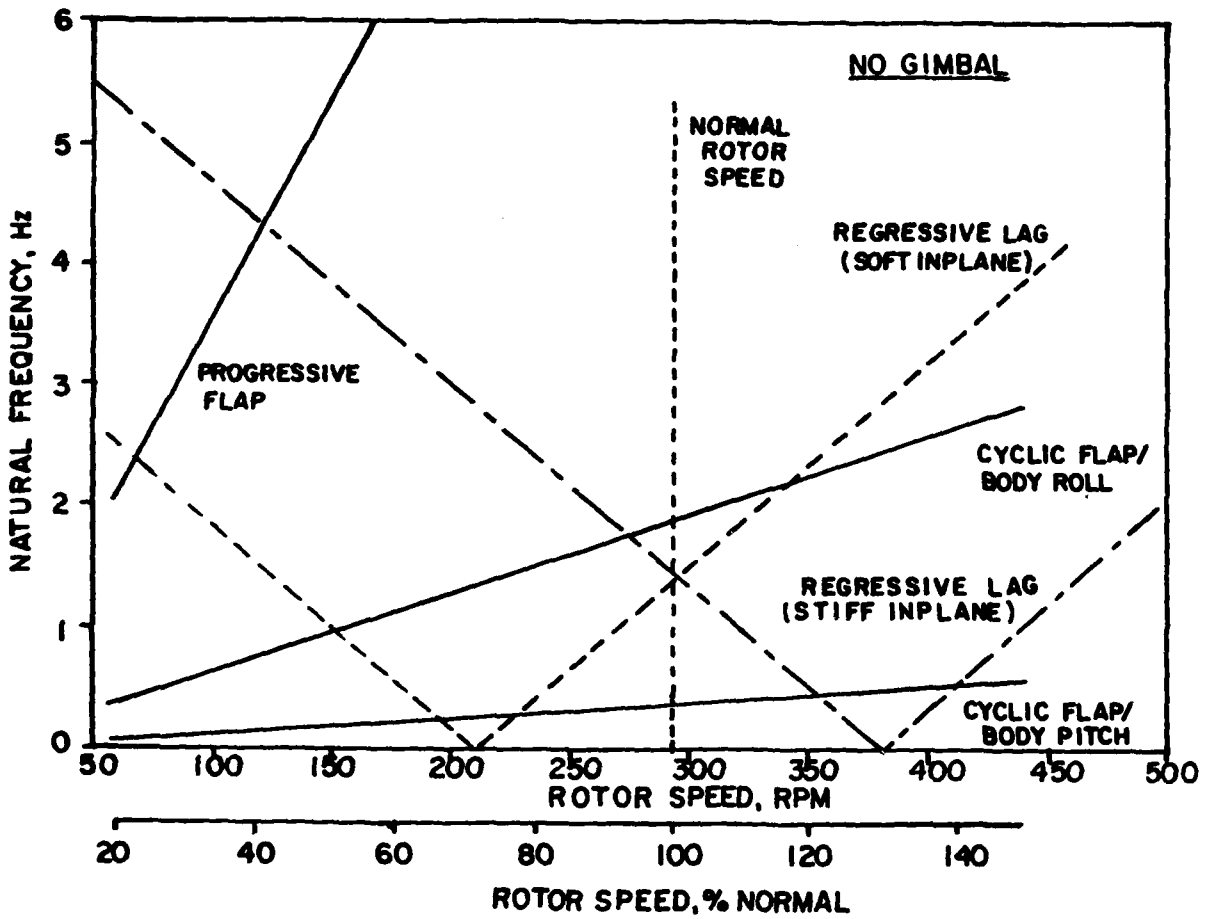

Figure 17. With No Gimbal DOF Body Modes are Separated From Lag Mode for Stability

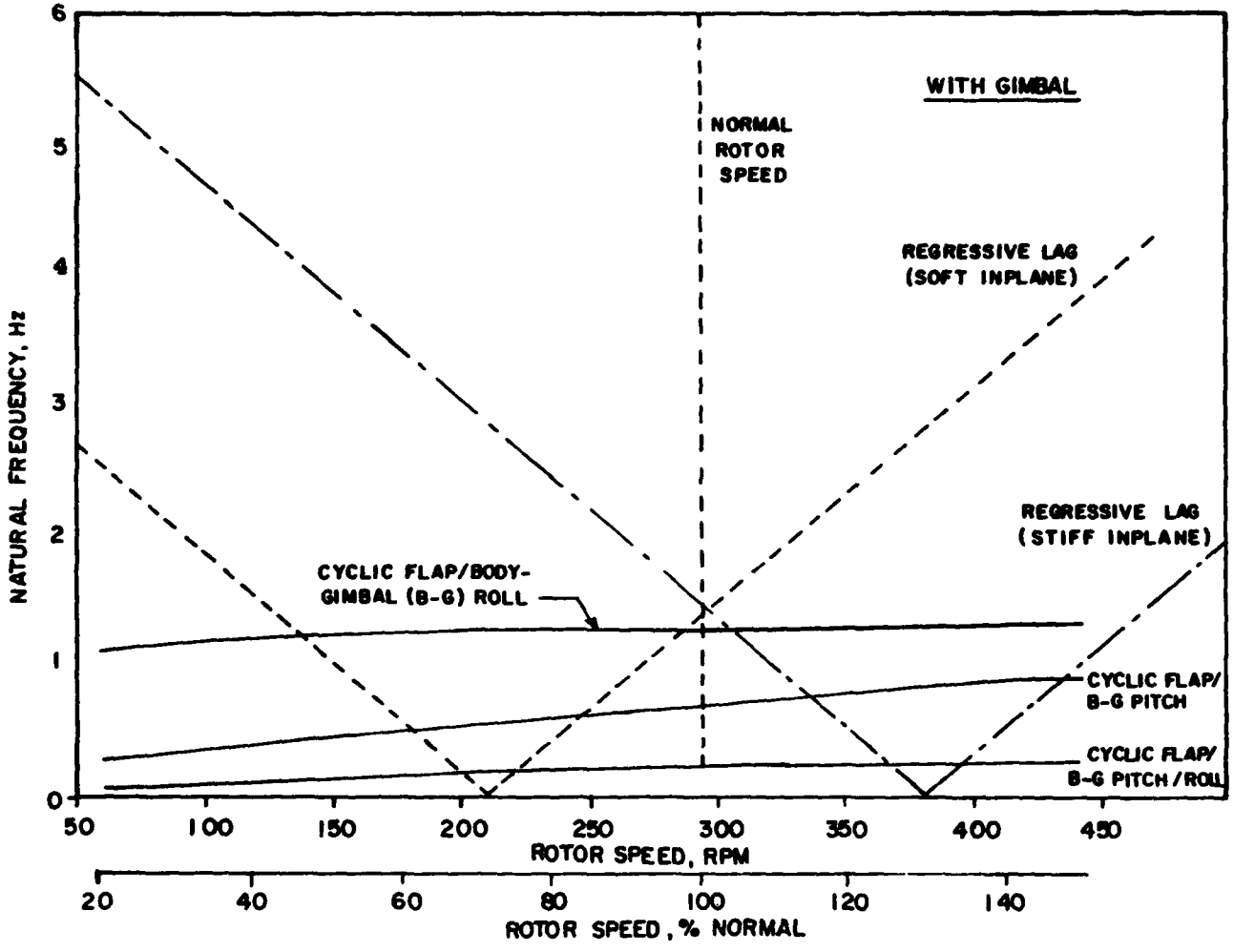

Figure 18. Gimbal DOF Causes Lag Mode to be Close to Body Roll Mode - Destabilizing

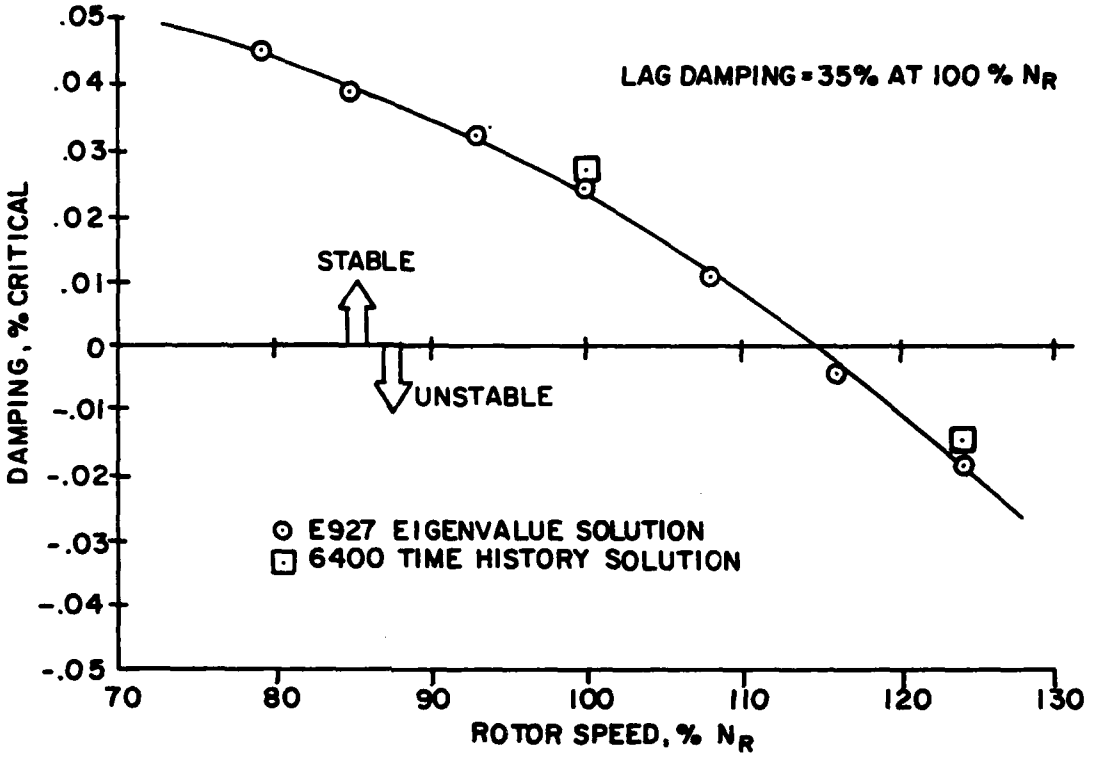

Figure 19. Ground Resonance Correlation

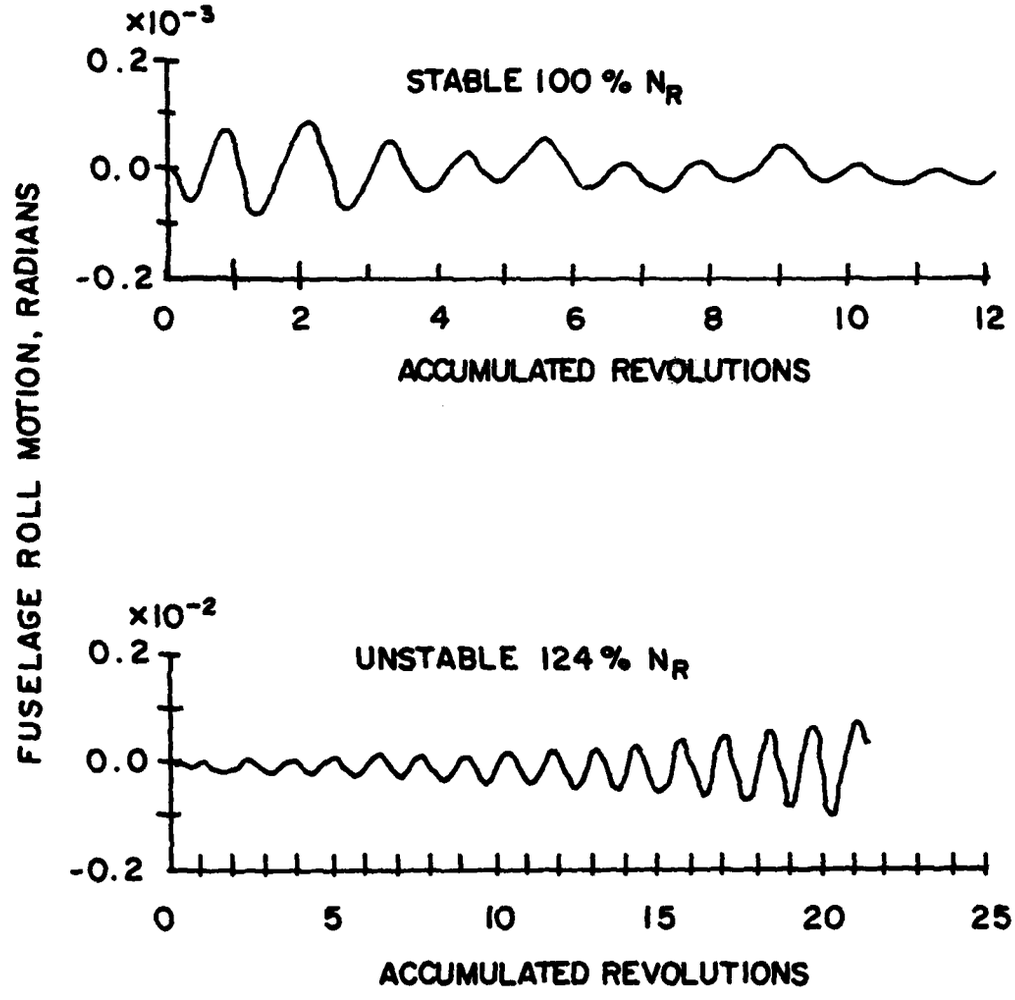

Figure 20. Ground Resonance Correlation Cases

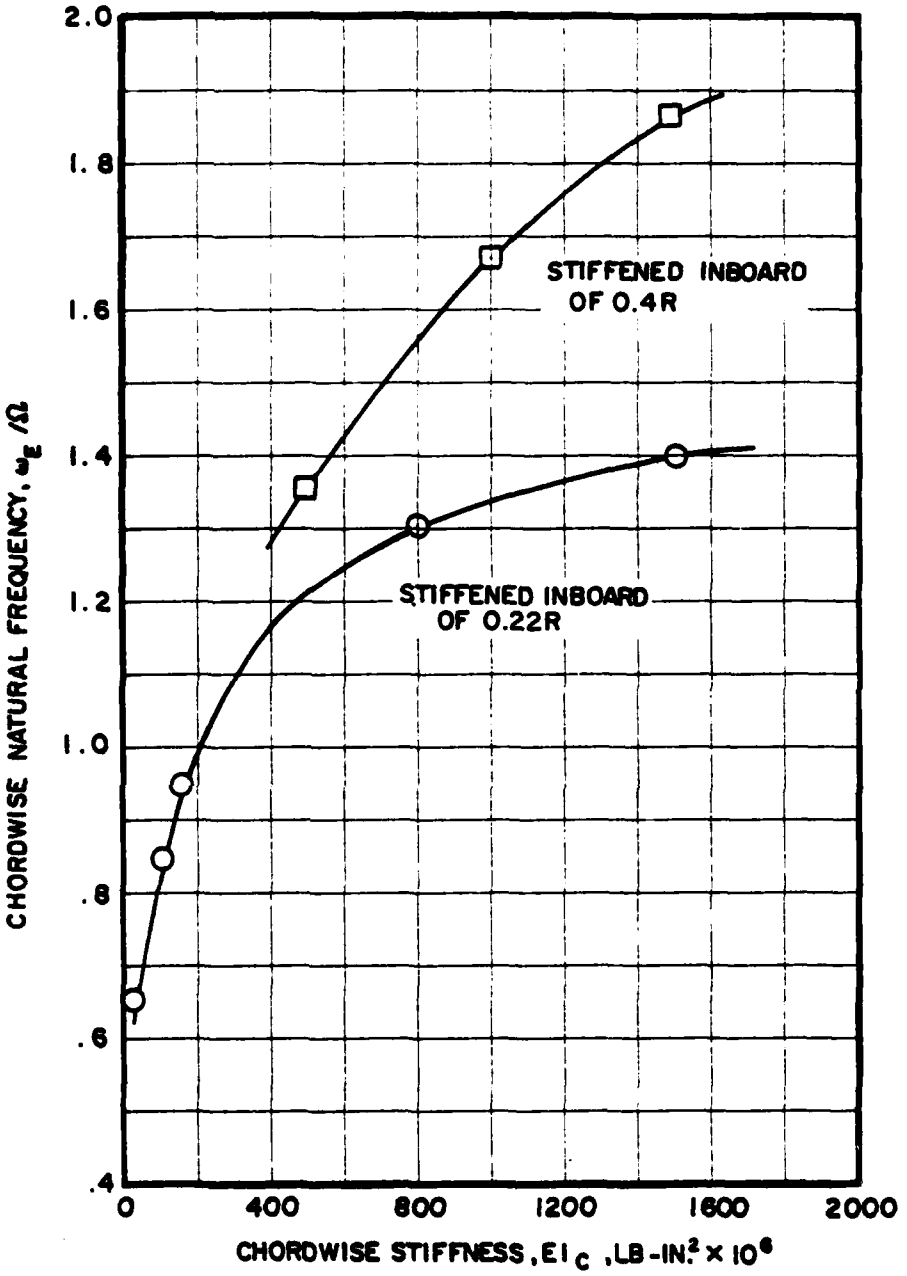

Figure 21. Effect of Chordwise Stiffness on Chordwise Natural Frequency

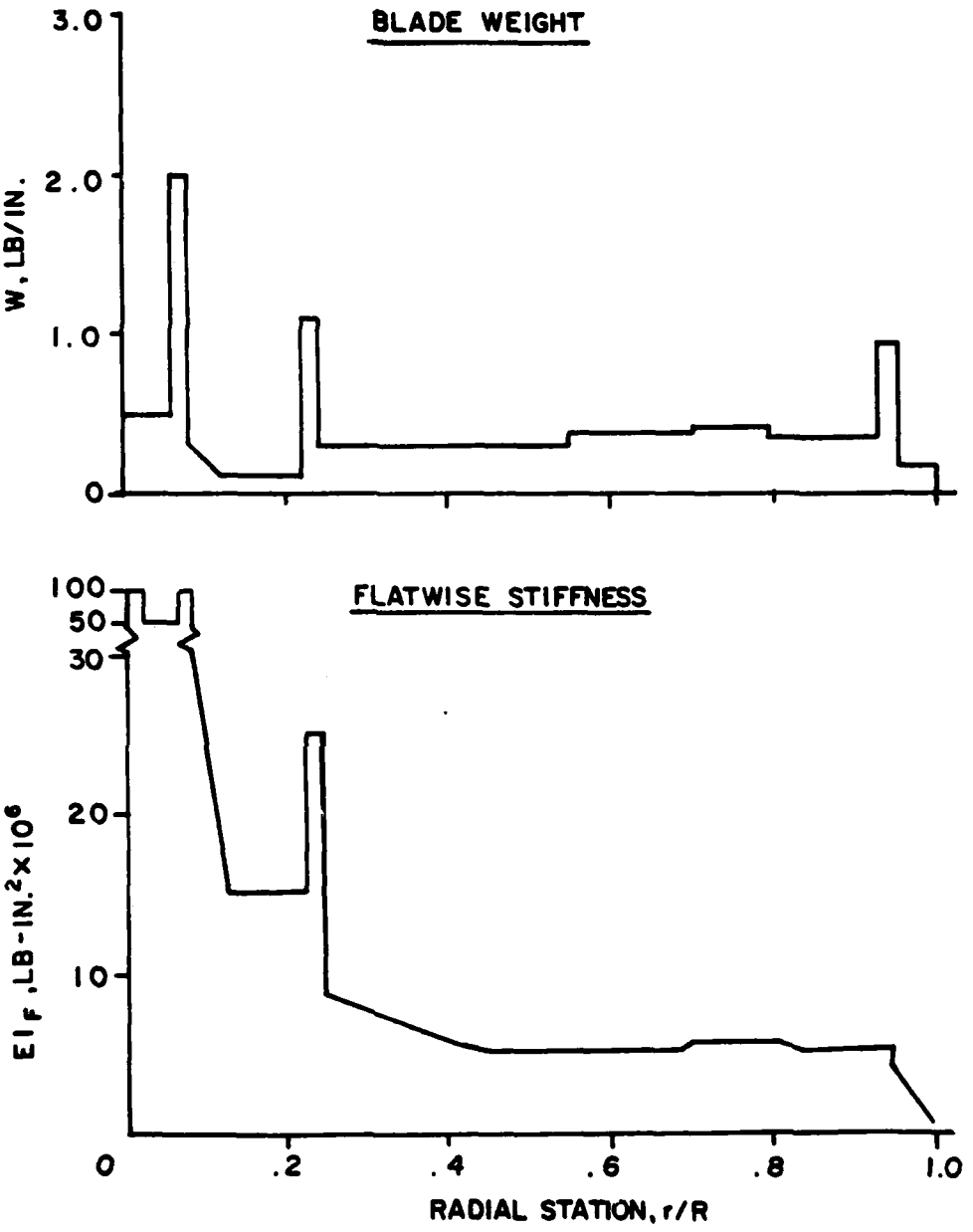

Figure 22. Blade Mass and Stiffness Properties

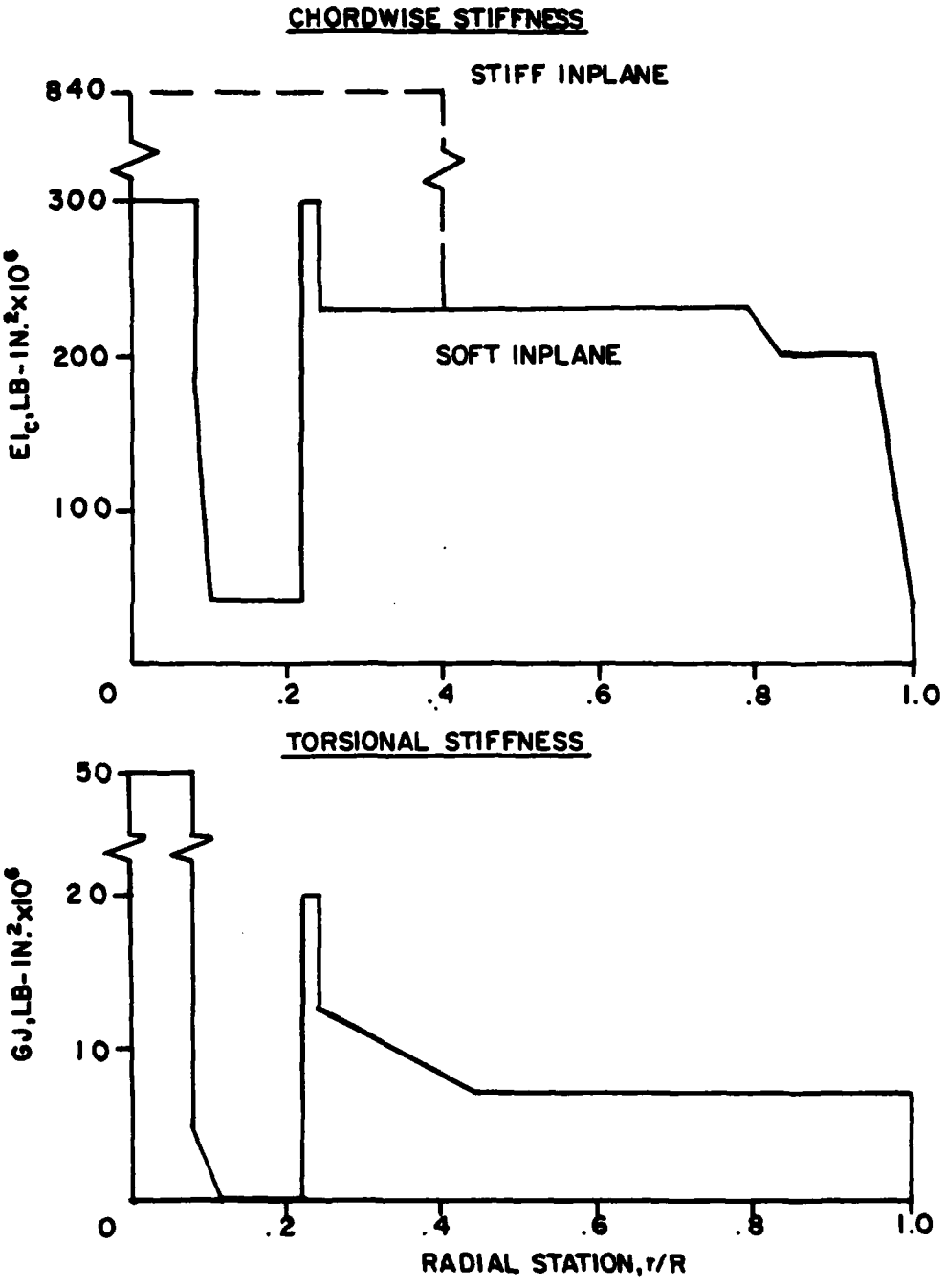

Figure 23. Blade Stiffness Properties

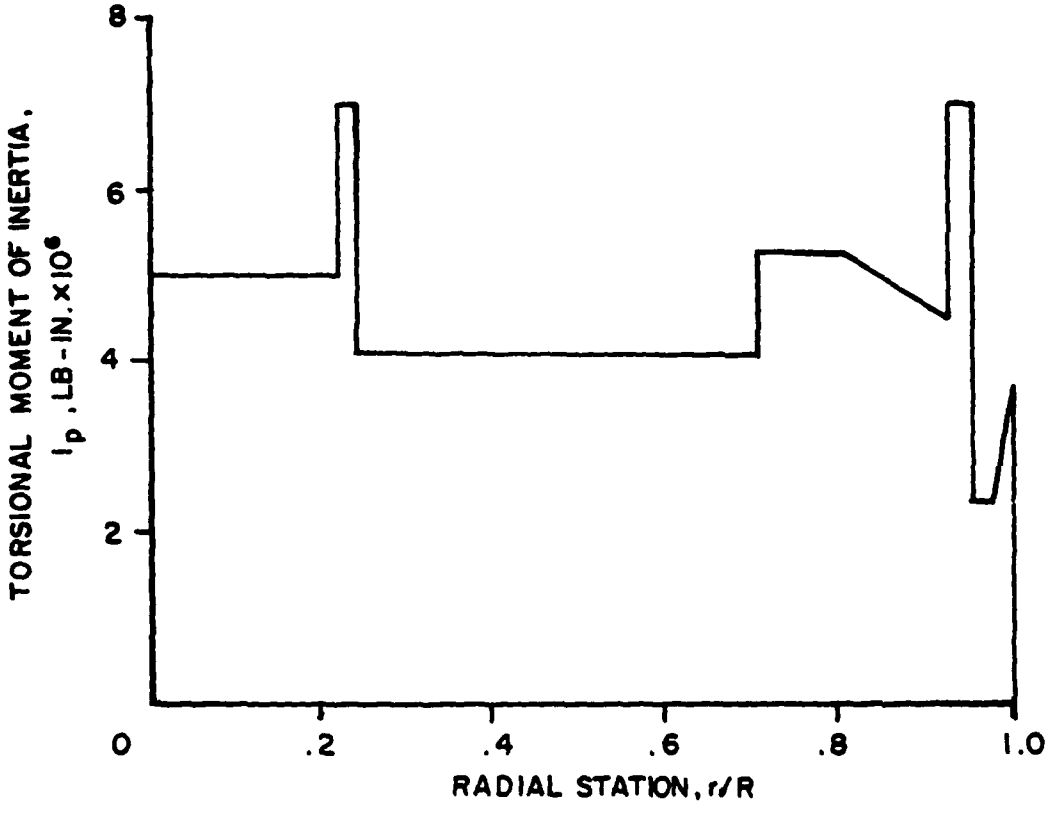

Figure 24. Blade Torsional Moment of Inertia Distribution

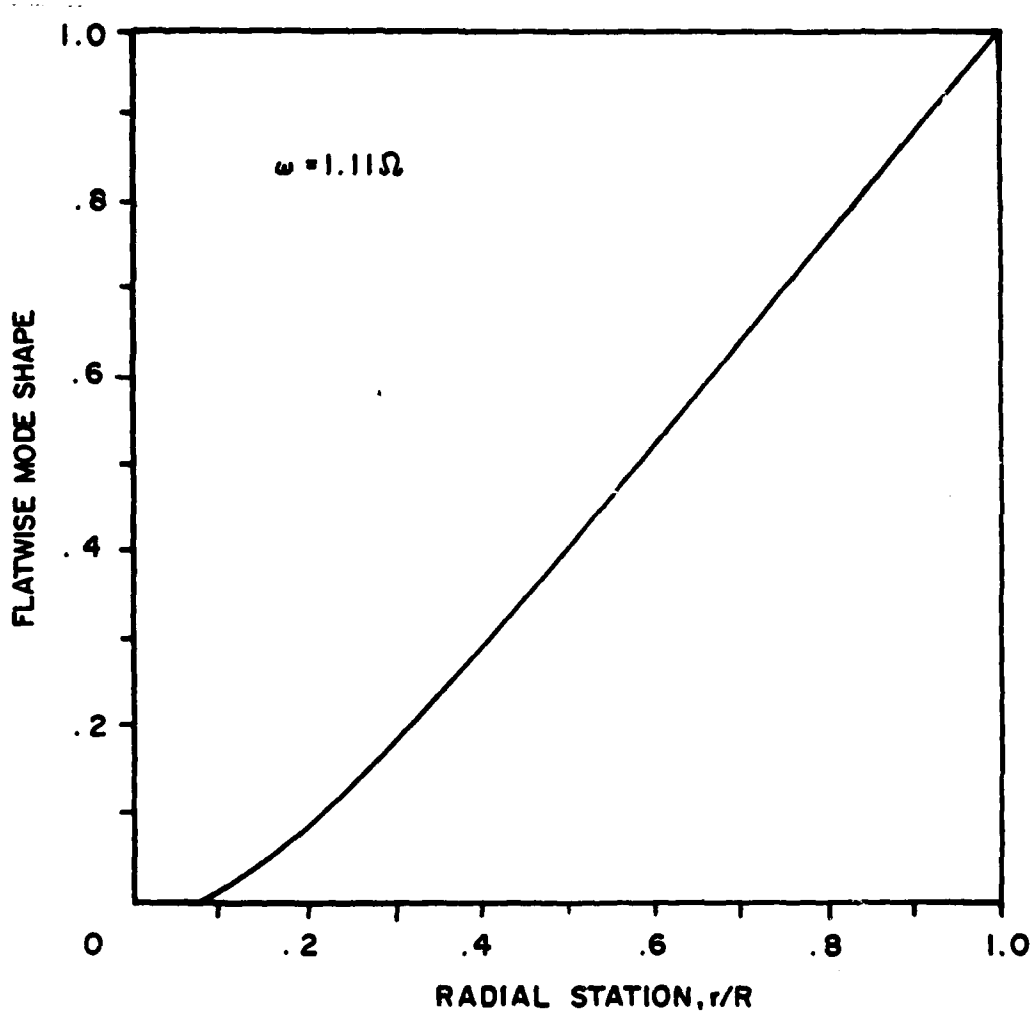

Figure 25. EGR Blade First Cantilevered Mode Shape: Flatwise

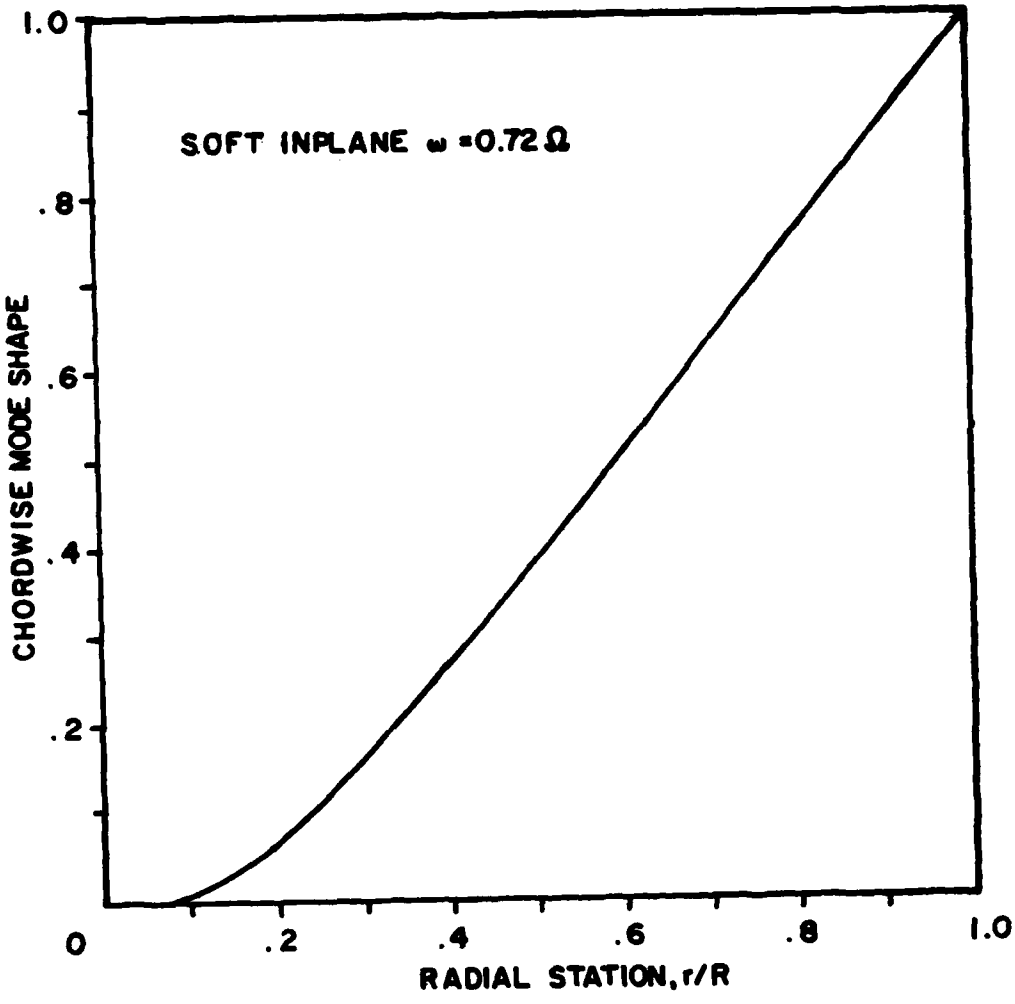

Figure 26. EGR Blade First Cantilevered Mode Shape: Chordwise

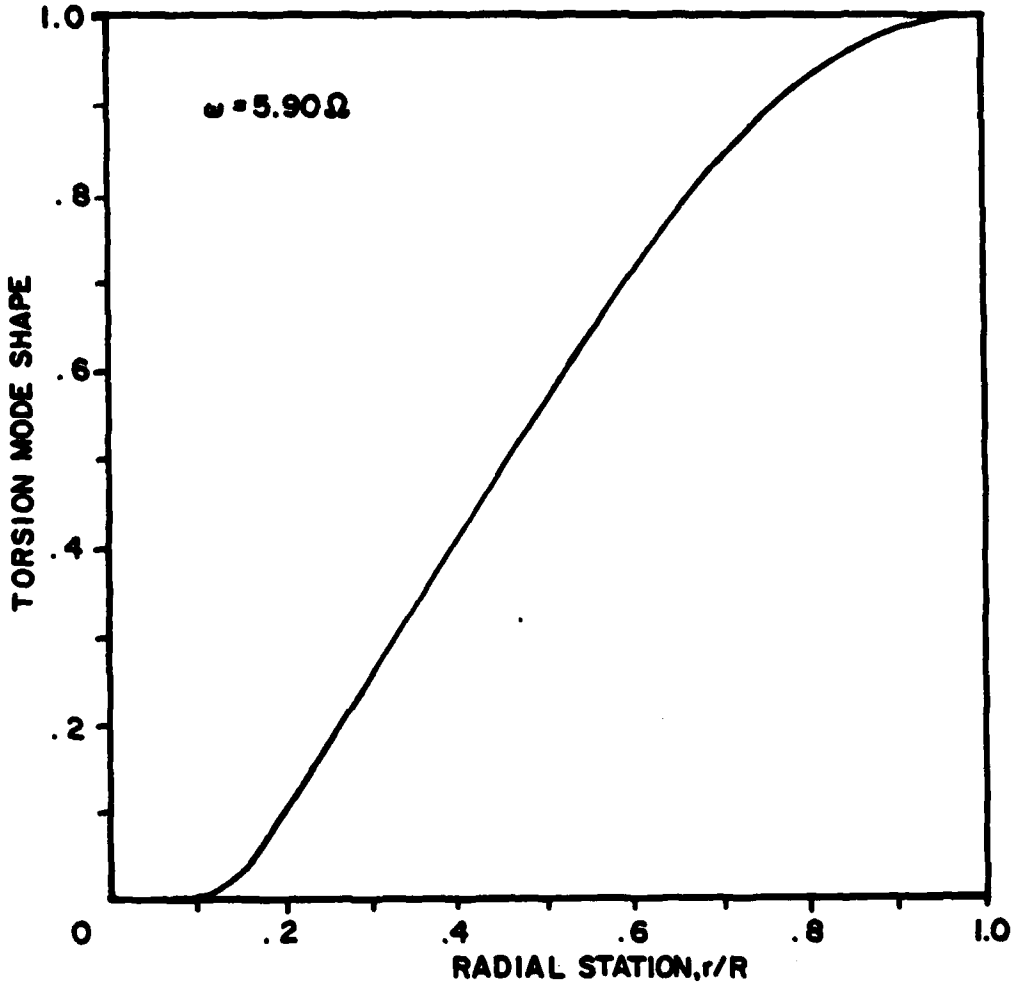

Figure 27. EGR Blade First Torsion Mode Shape (Rigid Root)

1. GIMBAL TILTS DUE TO UNBALANCED CF FROM CYCLIC LAG.

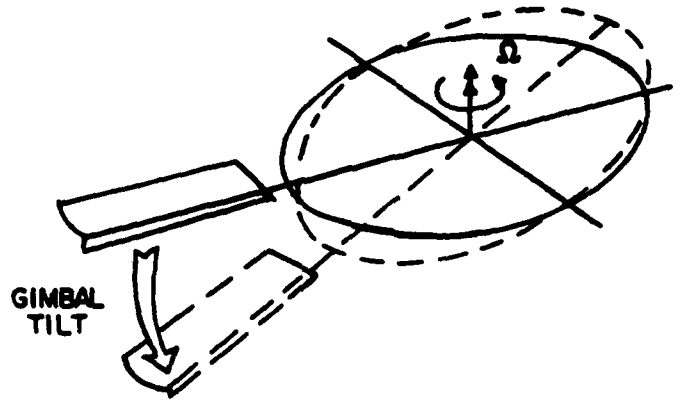

2. BLADE CYCLIC PITCH CHANGES DUE TO GIMBAL MOTION AND PUSHROD CONSTRAINT.

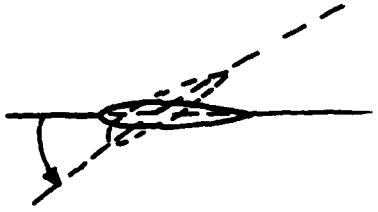

3. CYCLIC FLAPPING OCCURS DUE TO CYCLIC LIFT CHANGE INDUCED BY CYCLIC PITCH.

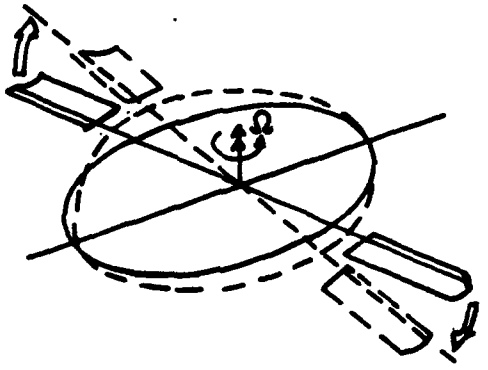

4. GYROSCOPIC MOMENT GENERATED DUE TO CYCLIC FLAPPING. THE MOMENT CAN BE EITHER IN THE DIRECTION OF ORIGINAL GIMBAL TILT OR OPPOSING THE TILT, DEPENDING ON THE CYCLIC FLAPPING CAUSED BY THE CYCLIC PITCH CHANGE.

Figure 28. Mechanism for Coupled Rotor-Gimbal Stability

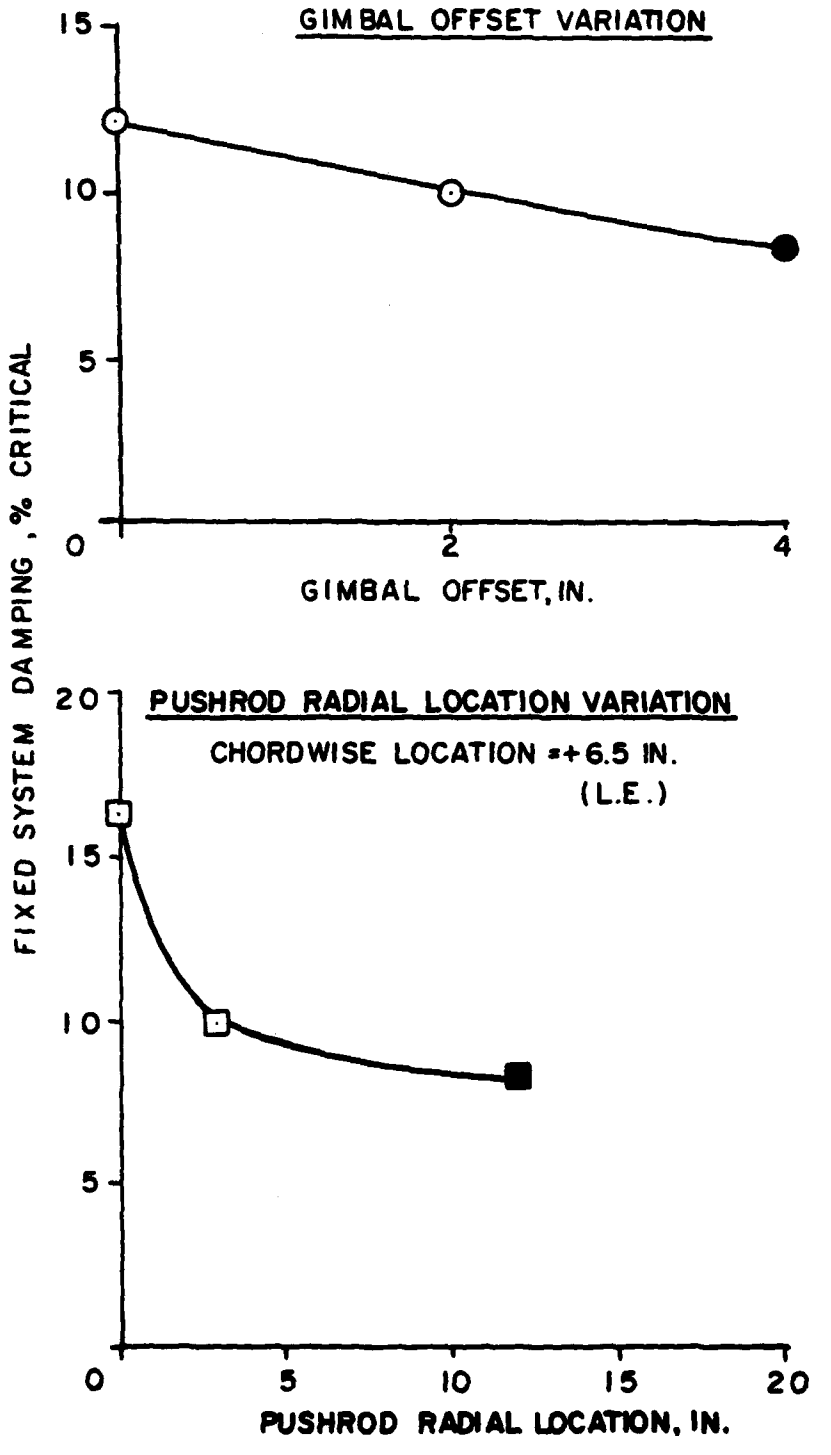

Figure 29. Hover Stability Gimbal Height and Push Rod Location Effects

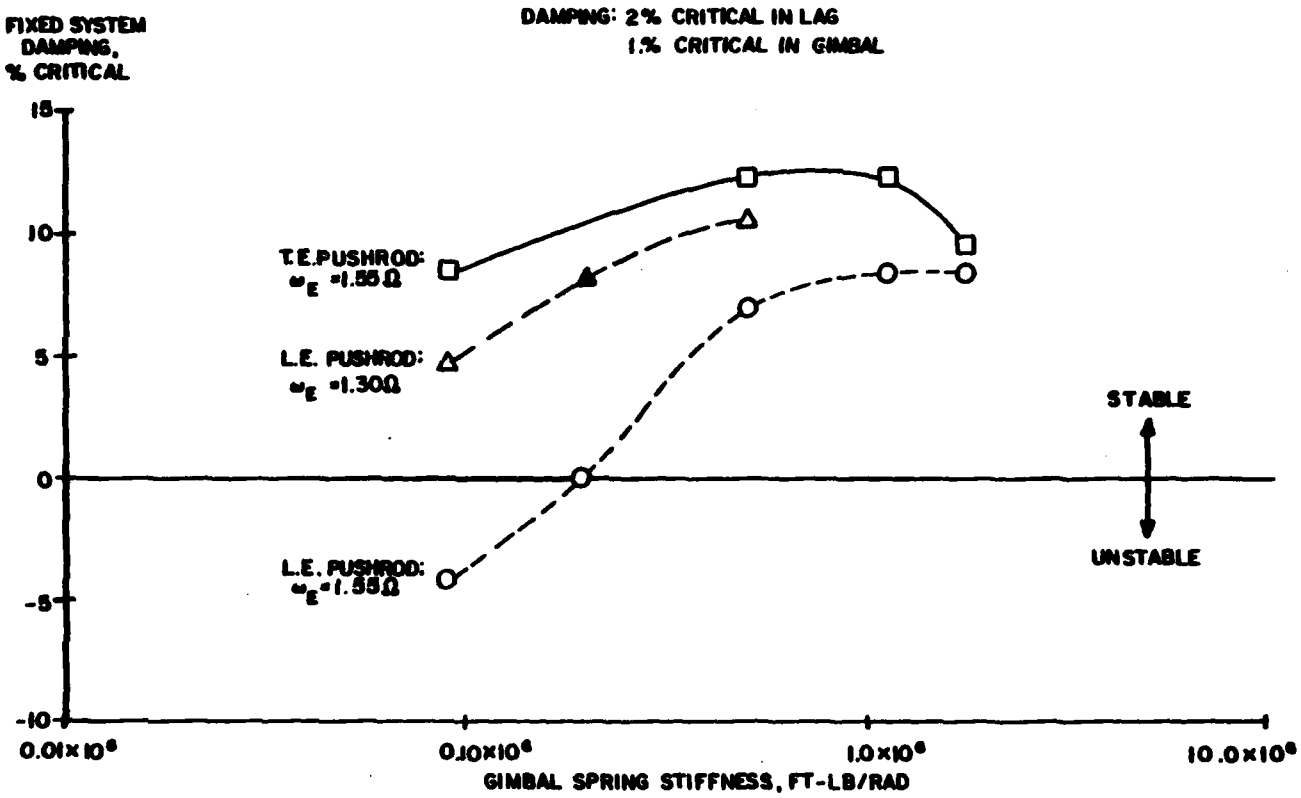

Figure 30. Gimbal Spring Stiffness Effects on Hover Stability

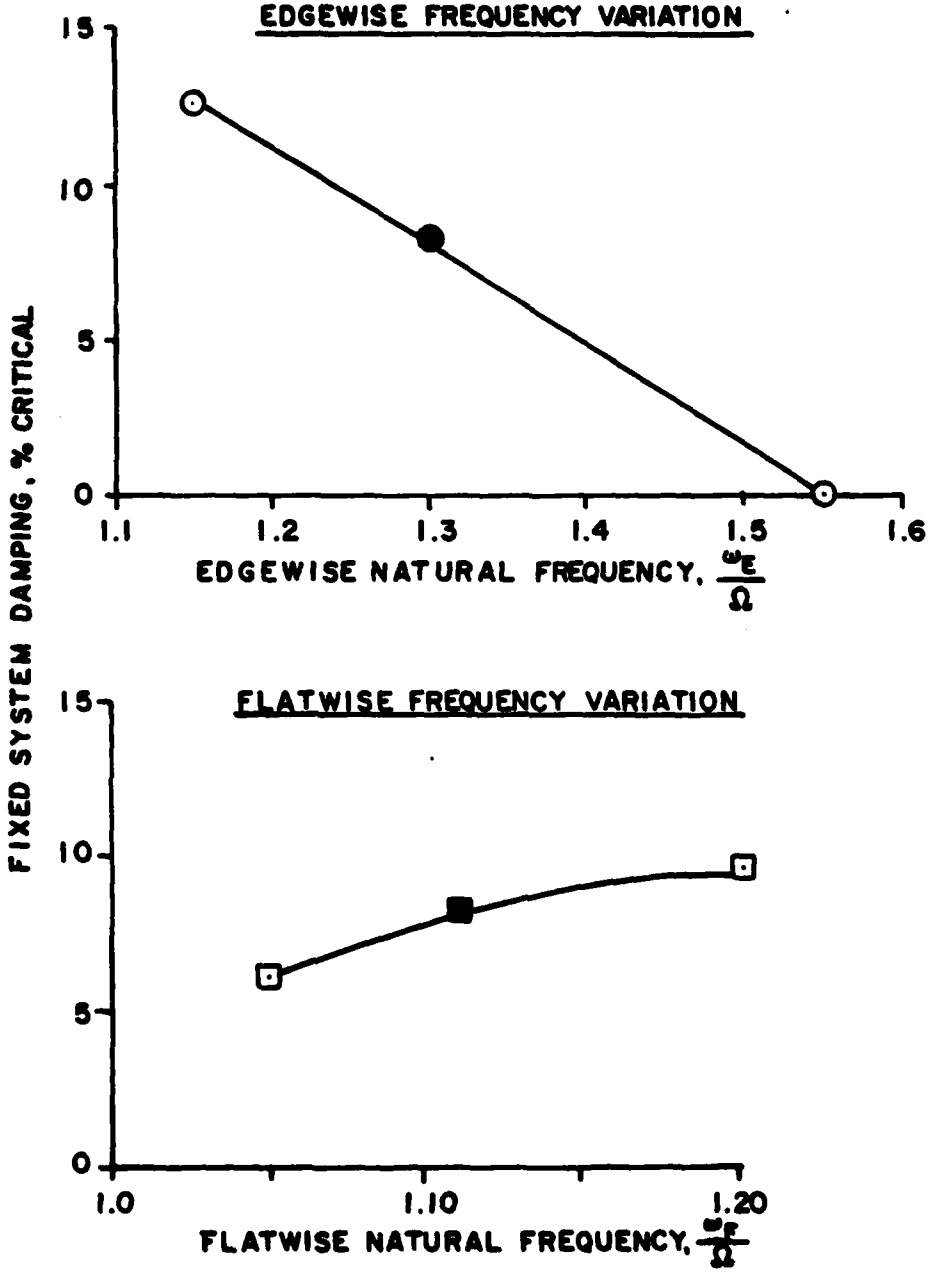

Figure 31. Effect of Blade Frequency on Hover Stability

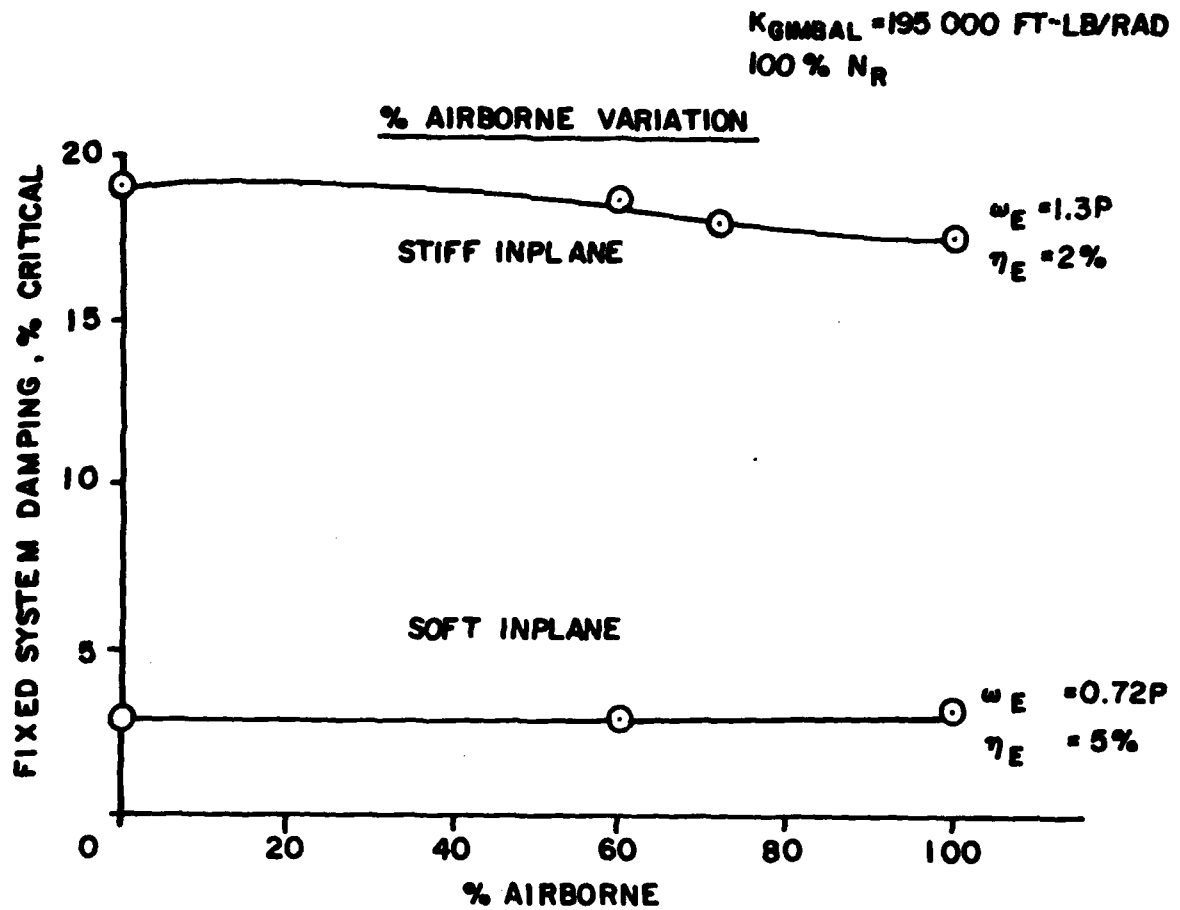

Figure 32. *Both Rotors are Stable for Ground* Resonance

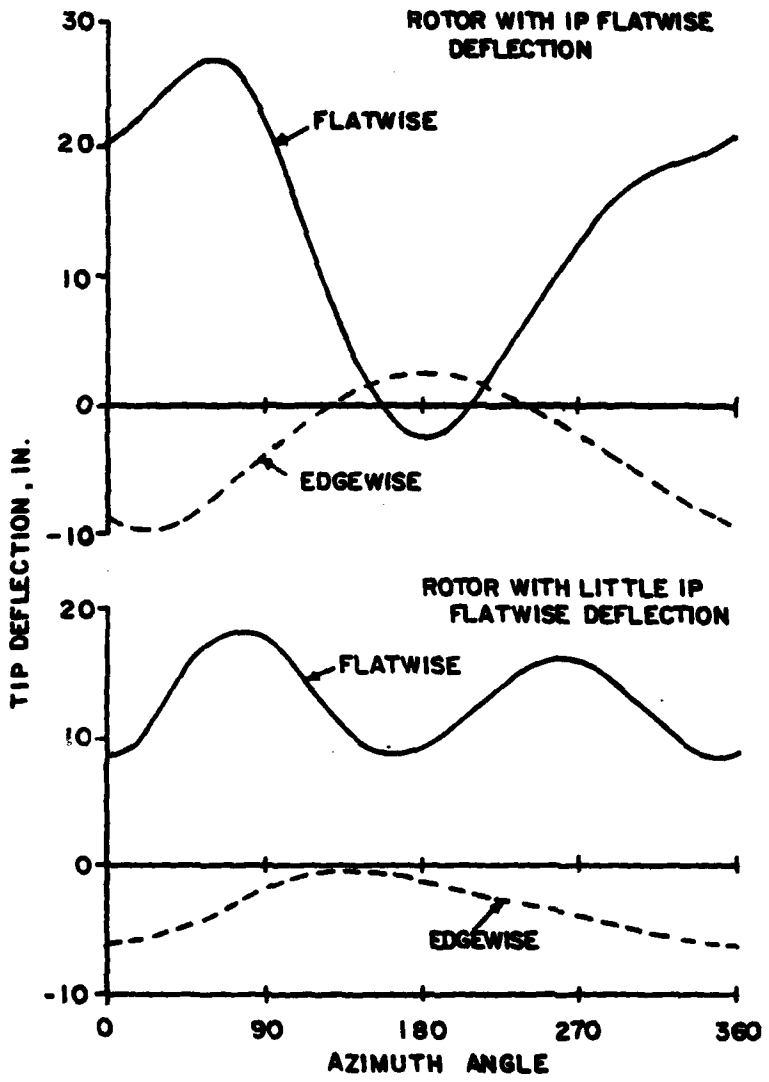

Figure 33. Effect of 1P Flatwise Response on Edgewise Response

1. Report No. NASA CR 166287 USAAVRADCOM TR 82-A-3	2. Government Accession No.	3. Recipient's Catalog No.
4. Title and Subtitle AEROELASTIC ANALYSIS OF THE ELASTIC GIMBAL ROTOR		5. Report Date May 1981 6. Performing Organization Code
7. Author(s) Raymond G. Carlson Wen-Liu Miao		8. Performing Organization Report No. SER-510048 10. Work Unit No.
9. Performing Organization Name and Address Sikorsky Aircraft Division of United Technologies Corporation Stratford, CT 06602		11. Contract or Grant No. DAAK51-80-C-0016
12. Sponsoring Agency Name and Address Aeromechanics Laboratory U.S. Army Research & Technology Laboratories (AVRADCOM) Moffett Field, CA 94035		13. Type of Report and Period Covered Contractor Report May 1980 - May 1981 14. Sponsoring Agency Code DAVDL-AL-RD

15. Supplementary Notes

Technical monitor: Robert A. Ormiston, Aeromechanics Laboratory, M/S 215-1
Contract administered by Applied Technology Laboratory, U.S. Army Research and Technology Laboratories (AVRADCOM), Ft. Eustis, VA 23604

16. Abstract

A preliminary aeroelastic and structural loads analysis of the elastic gimbal rotor (EGR) supported the feasibility of the concept. The Sikorsky elastic gimbal rotor is a new concept in helicopter rotors. It combines bearingless rotor blades with a gimballed hub which includes a spring element across the gimbal bearing. This provides the capability to select the desired control power or hub moment stiffness while maintaining the simplicity of bearingless rotor blades. The structural loads analysis of the elastic gimbal rotor indicated that the gimbal spring element is the critical component in the rotor system design, but that practical designs for all components should be achievable. The aeroelastic analysis was conducted using a version of the G400 Rotor Aeroelastic Analysis especially modified to evaluate the EGR. Hover stability showed that a stiff inplane blade was more stable than a soft inplane blade. Stability was sensitive to control system coupling (pitch-gimbal coupling), gimbal spring stiffness, and blade frequency placement. Ground resonance analysis showed both soft and stiff inplane rotors to be stable. A limited evaluation of the EGR in forward flight was conducted. Due to G400 analysis limitations, the results were not sufficient to define forward flight stability and stress limits. Continued development of the EGR concept is recommended, including model tests to confirm the concept feasibility and design requirements and to correlate with analysis.

17. Key Words (Suggested by Author(s))	18. Distribution Statement
Helicopters Helicopter Rotors Rotor Stability Rotor Loads Aeroelasticity	Unclassified - Unlimited STAR Category - 02

19. Security Classif. (of this report)	20. Security Classif. (of this page)	21. No. of Pages	22. Price*
Unclassified	Unclassified	105	

*For sale by the National Technical Information Service, Springfield, Virginia 22161